Real-Time Predictive Speed Control for Eco-Driving at Signalized Intersections Considering Queue Constraints

Eline M.C. Schropp

Master of Science Thesis

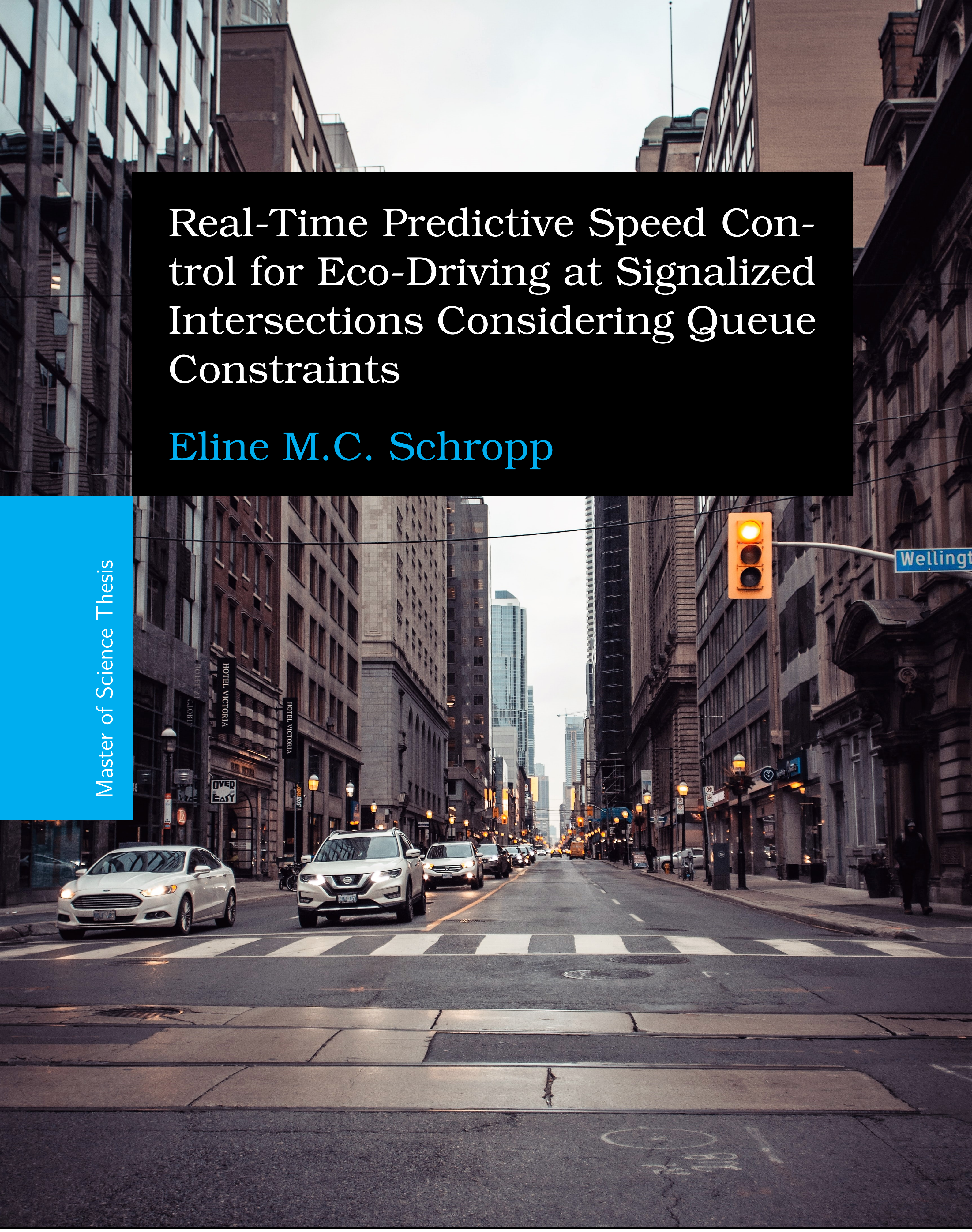

Delft University of Technology

Delft Center for Systems and Control

Real-Time Predictive Speed Control for Eco-Driving at Signalized Intersections Considering Queue Constraints

Master of Science Thesis

For the degree of Master of Science in Systems and Control at Delft University of Technology

Eline M.C. Schropp

July 7, 2022

Faculty of Mechanical, Maritime and Materials Engineering (3mE) · Delft University of Technology

Abstract

Speed trajectories considerably influence vehicular fuel consumption, particularly on signalized roads. To minimize fuel consumption, sharp acceleration/deceleration maneuvers and idling events at signalized intersections should be prevented. By taking advantage of the technological developments in infrastructure-to-vehicle communication, the possibility of receiving traffic signal phase and timing information in advance is enabled. Although a vast amount of research has been dedicated to optimal speed trajectory planning, existing methods may not be adequate in identifying the optimal solution for vehicles driving on signalized roads. Most studies do not involve queue estimation in the algorithm, which makes it challenging to deploy these methods in practice. Moreover, research efforts focus on undersaturated traffic conditions where queues can completely dissolve in a single cycle. Once the network is oversaturated, residual queues are formed generating traffic fluctuations and complete stops, significantly reducing the effectiveness of the application.

In this thesis, an optimal control problem is formulated to obtain the optimal speed trajectory, where traffic induced constraints are taken into account and queue estimation is explicitly integrated into the control framework. Based on kinematic wave theory, an efficient and accurate procedure to formulate the queue constraints in various traffic conditions is developed. To facilitate real-time control actions, the constrained optimization problem is solved using model predictive control. The simulation case studies show the proposed algorithm achieves vehicular fuel consumption savings as high as 29.15% compared to an existing approach in the literature. However, the fuel consumption savings are at the expense of an increase in travel time up to 1.65% compared to the literature approach. The results also indicate the benefits grow with increasing market penetration rates (MPRs) of controlled vehicles until it levels off at about 80% MPR. Furthermore, the results demonstrate the proposed algorithm can deal with stochasticity in traffic behavior. Finally, the thesis highlights the need for future research to further improve the proposed algorithm.

Table of Contents

List of Figures

List of Tables

Acknowledgements

With this thesis, I not only mark the end of my master's in Systems and Control but also the end of almost 8 years of studying at Delft University of Technology. Now that I have come to the beginning of the end, this thesis has not progressed as expected due to the global corona pandemic. I never imagined the end of my student life concluding the way it did, but I am grateful for all the things I accomplished in those remarkable years.

In the first place, I would like to thank my supervisors Azita Dabiri and Paul van Erp for providing constructive and detailed feedback, asking questions that pushed me in the right direction, thinking along and for all the time invested in my growth.

In addition, I would like to thank my family for believing in me and supporting me with their comments and auxiliary support like office space during this difficult last phase of my studies.

Finally, I would like to thank my friends with whom I completed projects, studied for the exams and joined the occasional Lagerhuysch drinks. All these people contributed to my thesis in some shape or form and without their help, I would have been unable to complete the project.

Delft, University of Technology — Eline M.C. Schropp
July 7, 2022

Chapter 1

Introduction

As a result of increasing economic activities and a growing population, interrupted and congested traffic flow presents a significant problem on signalized roads. Longer travel times and idling increase fuel consumption, which in consequence harms the environment due to the emission of greenhouse gasses (GHG). According to Byrne et al. [1] urban traffic in Germany in 2018 was accountable for approximately 43% of nitrogen oxides (NO_x) emissions and 33% of carbon monoxide (CO) emissions. Furthermore, as oil consumption grows, the shortage of fossil energy becomes severe. According to studies, at the current consumption rate oil will be depleted in roughly 35 years [2]. Hence, it is of great importance to reduce fuel consumption and emissions. Recently, studies attempted reducing fuel consumption and the emission of GHG by facilitating drivers with driving behavior instructions [3, 4], variable speed limit control [5], fuel-optimal vehicle platooning [6] and environmental friendly routing [7]. All these studies have in common that a vehicle can significantly reduce fuel consumption and GHG emissions if it follows the provided optimal speed trajectory.

With the rising awareness of the relation between speed, acceleration, deceleration and fuel consumption, many studies focus on applying optimal speed control to vehicles. For highways, the relation between speed profiles, fuel consumption and emission rates has been extensively studied [8]. Highways have no traffic signals that bring traffic to a complete standstill and therefore have a continuous traffic flow. Consequently, vehicles on highways have no constraints on the time interval at which they have to reach a specific location on the road, which makes it relatively straightforward to create optimal speed algorithms by adjusting the behavior of drivers.

Novel studies therefore focus on applying optimal speed trajectory control to vehicles driving on signalized roads. A common objective of these research efforts is to provide drivers with an optimal speed profile to prevent sharp acceleration/deceleration maneuvers and reduce idling time, which are the primary causes of high fuel consumption. For instance, American drivers spend on average a total of 54 hours in congestion and waste 21 gallons of fuel at a cost of 1080 dollars in wasted fuel per year [9]. A considerable share of this idling time is spent in front of traffic lights. Poor signal timing is responsible for an estimated 10% of all delays on urban roads [10]. Advanced traffic signal control mechanisms such as signal synchronization and traffic-actuated signals have been installed at intersections, saving time and fuel. However, such measures are expensive to implement and maintain [11] and even with these measures, drivers frequently travel at full speed towards a green light and must come to a complete stop when the signal turns red. The absence of information about the traffic signal's future state increases travel time, fuel consumption and emissions [12]. In an ideal scenario, the future phase and timing of a traffic signal are known and the driver can adjust its speed for arrival during a green phase.

1-1 State of the art

Recently, research has been conducted on developing optimal speed planning models based on standardized traffic signal phase and timing (SPaT) information. With the developments in infrastructure-to-vehicle (I2V) communication, it is possible to receive the current phase and timing of traffic signals in advance. Based on this information it is possible to apply speed control to the vehicle, reducing the likelihood of stopping and idling in front of the red traffic light. In addition to maximizing the probability of passing a green light, the cost function can be chosen such that it reduces fuel consumption and emissions. Hence, instead of changing the design of the timing controller of the traffic signal, optimal speed planning methods can be designed that take state and input constraints into account while simultaneously minimizing fuel consumption and/or emission rates.

In this thesis, the focus will be on speed trajectory control of individual vehicles driving on a single-lane signalized road. Only single-lane roads are considered, where both the upstream and downstream roads merely consist of one lane. This ensures vehicles do not overtake their leader and that there is no lane-changing behavior. This assumption is made to prevent dealing with complex lane-changing characteristics and is reasonable since urban lane changes have not been extensively studied [13].

Speed trajectory control for individual vehicles is currently addressed using several approaches like dynamic programming (DP) [14, 15], model predictive control (MPC) [16, 17] or other optimization-based approaches [18, 19]. While current methods, such as DP, can obtain the global optimum strategy over the entire driving route, they require complete knowledge of the traffic conditions in advance [20]. Specifically, DP is based on a time domain and after any divergence from the optimal strategy, the remaining profile needs to be completely optimized again. The computation time of DP is therefore extremely dependent on the number of discretized states. Because of this limitation, such an approach is only used in offline and pre-trip scenarios under the assumption of free-flow traffic conditions [21]. Alternative methods for eco-driving decrease their computation time by optimizing over a finite prediction horizon and repeating the optimization process at every time step like MPC [22].

MPC is a model-based control method that utilizes a dynamic model to predict system behavior and repeatedly calculate the optimal control sequence online in a receding horizon way. MPC is one of the model-based control strategies that is currently attracting research attention and is widely implemented in a variety of industrial fields [23]. MPC represents a promising method for speed trajectory control of vehicles in urban areas since: (i) it can optimize over a combination of objectives like fuel consumption, control effort, emission rates and travel time of the individual vehicles; (ii) through the receding horizon procedure, MPC can work with real-time feedback which makes it robust against uncertainties of the process; (iii) traffic induced restrictions can be included as MPC can take state and input constraints into account; (iv) MPC is modular allowing the prediction model to be selected and substituted based on the trade-off between computational efficiency and accuracy or the control objectives.

1-2 Scientific gap

Although a vast amount of research has been dedicated to optimal speed trajectory planning, existing methods may not be adequate in identifying the optimal solution for vehicles driving on signalized roads. Most studies minimize fuel consumption and reduce idling time by only considering the constraints imposed by traffic signals. Nonetheless, idling time is also determined by the vehicle waiting queue and ignoring the spatial and temporal constraints by other road users could result in suboptimal or even infeasible solutions.

To consider the impact of surrounding traffic, Wang et al. designed a cluster-wise cooperative eco-driving strategy in a (partially) connected vehicle environment [24, 25]. He et al. [18] and Wu et al. [26] calculated optimal vehicle trajectories for individual vehicles while taking vehicle queues into account. However, the studies above assumed that the queuing process can be detected with on-board sensors, can be predicted based on historical data or is known in advance. These assumptions are not entirely realistic as the length of the queue changes over time and can be difficult to detect especially when the penetration rate of connected vehicles is relatively low. Therefore, without involving queue estimation in the algorithm, it will be quite challenging to deploy these methods in practice. Yang et al. [27] estimate the queue length ahead of the controlled vehicle and ensure it arrives at the intersection just as the last vehicle in the queue is released. However, this research effort focuses on undersaturated traffic conditions where queues can completely dissolve in a single cycle. Once the network is oversaturated, residual queues are formed generating traffic fluctuations and complete stops for the controlled vehicle, significantly reducing the effectiveness of the application.

1-3 Research objective

MPC has shown promising results in the control of vehicles driving on signalized roads and the computation time has the potential to be fast enough for real-time implementation. Therefore, the main goal of this thesis is:

> To develop a real-time implementable predictive speed control (PSC) strategy for vehicles proceeding through signalized intersections to reduce fuel consumption while considering queue constraints.

One of the main challenges lies in the accuracy of estimating queue propagation in real-time and efficiently integrating the queue constraints into the control framework. Consequently, the following subquestions are formulated to achieve the main research objective:

1. *What is an accurate method to estimate queue propagation in the vicinity of signalized intersections?*

In principle, one can predict the queuing effect and derive the spatial and temporal restrictions by using microscopic car-following models or macroscopic traffic flow models.

2. *How can the queue constraints be integrated into the control framework such that it operates in various traffic conditions?*
   In fact, the effectiveness of the optimal speed profile provided by the PSC strategy depends heavily on the estimation efficiency and accuracy of signal and traffic conditions.

The unique contribution of this thesis is the use of MPC to provide real-time speed advice for vehicles driving on a single-lane signalized road taking into account traffic induced constraints and explicitly involving queue estimation in the algorithm. The developed algorithm is a general framework and can be used in various traffic conditions, varying from undersaturated to oversaturated.

1-4 Thesis outline

The remainder of this thesis is organized as follows. Chapter 2 presents an overview of the relevant background information and preliminaries regarding traffic flow modelling and speed trajectory control on signalized roads. In Chapter 3, a vehicle model is developed, which is then used to identify the optimal problem formulation. The effectiveness of the Eco-PSC algorithm is evaluated and analyzed by running different simulation case studies in Chapter 4. Finally, Chapter 5 concludes this thesis together with recommendations for future research.

Chapter 2

Background and preliminaries

In this chapter, relevant literature and theories are discussed to establish the basis upon which the rest of this thesis is built. In order to achieve this, fundamental traffic flow theory is detailed at the beginning of this chapter. Different levels at which traffic is typically described are discussed by means of the primary variables in Section 2-1. Section 2-2 illustrates the basic concept of kinematic wave theory. This section further elaborates on how kinematic wave theory can be deployed to determine the cumulative number of vehicles. Subsequently, the effects of queues and vehicle spillback on signalized roads are discussed in Section 2-3. Lastly, the concept of model predictive control (MPC) is introduced in Section 2-4, which is used as the control framework in this thesis.

2-1 Traffic variables

Different levels of detail can be distinguished to describe the traffic conditions in a network. On a microscopic level, the characteristics of all individual vehicles are described to represent the traffic conditions. The main variables in this description are the time headway h, distance headway or spacing s and individual vehicle speed v [28]. The time headway is defined as the time it takes for the follower to reach the position of its leader. Similarly, the distance between the follower and its leader is defined as the spacing. Finally, the individual speed

Table 2-1: Outline of the traffic variables and their relationships, where the brackets specify the mean.

Microscopic	Symbol	Unit	Macroscopic	Symbol	Unit	Relation
Time headway	h	s	Flow	q	veh/h	$q = \frac{3600}{\langle h \rangle}$
Spacing	s	m	Density	ρ	veh/km	$\rho = \frac{1000}{\langle s \rangle}$
Individual speed	v	m/s	Average speed	u	km/h	$u = 3.6\langle v \rangle$

of a vehicle is defined as the distance traveled per unit of time. On the macroscopic level, the variables are aggregated and describe the characteristics of traffic as a whole. The traffic conditions on this level are described by the variables flow q, density ρ and average speed u [28]. The flow is specified as the number of vehicles passing a reference point per unit of time. The density is the number of vehicles per unit of road segment. Lastly, one can define the average speed of the vehicles in the network. The traffic variables and their relationships are summarized in Table 2-1.

2-1-1 Three-dimensional representation

A complete macroscopic description of traffic flow can alternatively be described using the three dimensions: space s, time t and cumulative flow $N(s,t)$ [29]. The cumulative flow describes the number of the last vehicle to pass location s before time t and is only applicable to traffic in one direction. As a result, this function is an integer variable and only grows over time. Technically speaking, the cumulative flow is a step function that increases with one every time a vehicle passes. However, for higher flow rates and longer periods, the function is frequently smoothed into a continuously differentiable function [28]. If $N(s,t)$ is smoothed and continuously differentiable, the partial derivatives of the cumulative flow with respect to time and space are the flow and (negative) density functions:

$$q(s,t) = \frac{\partial N(s,t)}{\partial t} \tag{2-1}$$

$$\rho(s,t) = \frac{-\partial N(s,t)}{\partial s} \tag{2-2}$$

The negative sign in Eq. (2-2) arises due to the convention that $N(s,t)$ is numbered in decreasing order in the direction of increasing s, see Figure 2-1. Assuming that the cumulative flow and its first and second derivatives exist, the identity

$$\frac{\partial^2 N(s,t)}{\partial s \partial t} = \frac{\partial^2 N(s,t)}{\partial t \partial s} \tag{2-3}$$

combined with Eq. (2-1) and Eq. (2-2) becomes:

$$\frac{\partial \rho(s,t)}{\partial t} + \frac{\partial q(s,t)}{\partial s} = 0 \tag{2-4}$$

which is better known as the conservation law. Solutions of the conservation law represent the evolution of a traffic state over space and time. Generally, the conservation law is expressed with regard to the cumulative flow [30].

In some circumstances, the difference in cumulative flow between two points in space-time has a physical meaning. To illustrate, the difference in cumulative flow between the upstream and downstream link boundary at time t yields the number of vehicles on the link. In Figure 2-1, the number of vehicles on the link at time t_3 is equal to the change in cumulative flow over the green line. Furthermore, the change in cumulative flow over the blue line is equal to

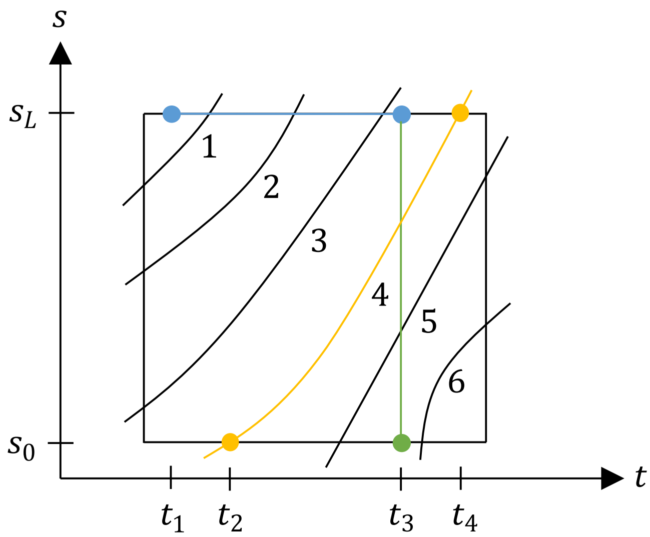

Figure 2-1: Vehicle trajectories, values for the cumulative flow function and change in cumulative flow between two points in space-time. The green line represents the number of vehicles that are present on the link at time t_3. The blue line represents the number of vehicles that have left the link between t_1 and t_3. The yellow line represents the travel time associated with the fourth vehicle, i.e. $t_4 - t_2$.

the number of vehicles that have left the link between t_1 and t_3. Lastly, the time difference between an equal value of the upstream and downstream cumulative flow curve determines the travel time associated with a specific vehicle number. For example, the travel time for the vehicle number related to the yellow curve is $t_4 - t_2$.

2-2 Traffic flow models

When selecting a traffic flow model for restriction calculations, it is important to make a trade-off between model accuracy and complexity. The choice between a microscopic and a macroscopic model primarily determines the complexity of the traffic flow model. In case of microscopic models, computer memory presents the limiting factor, as these models have to store data for all the individual vehicles in the network which significantly increases for large networks. Macroscopic models are faster in computation time and easily scalable as the number of variables is independent of the number of vehicles in the network. Consequently, estimating traffic constraints macroscopically is more useful in practice concerning data availability, scalability and computational efficiency. This, in addition, offers more possibilities to deal with non-deterministic factors (e.g. stochasticity in traffic behavior) and later expansion such as controlling multiple vehicles and traffic-actuated signals.

2-2-1 The LWR-model and kinematic wave theory

The basic concept behind all continuum macroscopic traffic flow models is the conservation principle derived from fluid theories. Recall that the conservation of vehicles was defined as:

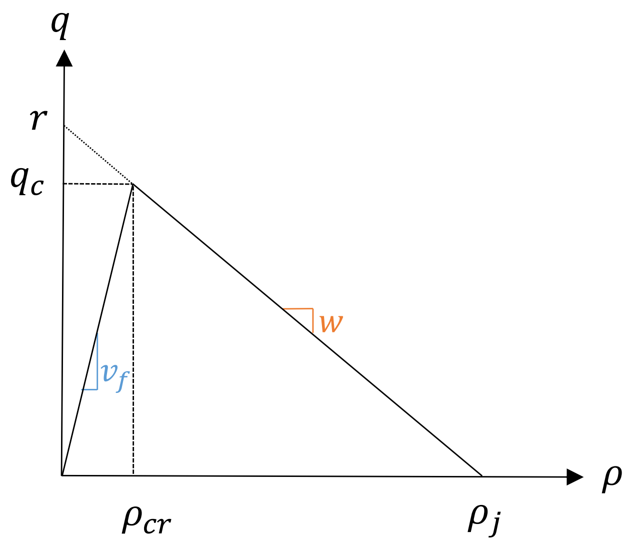

Figure 2-2: Triangular shaped continuous concave fundamental diagram with important parameters: free-flow speed v_f, capacity q_c, critical density ρ_{cr}, passing rate r, wave speed w and jam density ρ_j.

$$\frac{\partial \rho}{\partial t} + \frac{\partial q}{\partial s} = 0 \tag{2-5}$$

The kinematic wave theory (KWT), as originally described by Lighthill, Whitham and Richards [31, 32], arises from the assumption that in steady-state conditions a relationship between the flow q and density ρ exists, i.e.

$$q = Q(\rho) \tag{2-6}$$

This relation is the so-called fundamental diagram (FD) of traffic flow. In general, the flow is a continuous and concave function of the density.

Figure 2-2 shows a triangular shaped continuous concave FD. The triangular FD is extensively used in traffic state estimation because of its simplicity, theoretical preferable features and certain empirical evidence [33]. Traffic states on the left-hand side hold for vehicles travelling with free-flow speed v_f, whereas traffic states on the right-hand side are congested and travel with wave speed w. Free-flow states typically travel in the direction of traffic with a positive wave speed, as the slope of the tangent line is positive for the free-flow branch. In contrast, congested traffic states travel against the direction of traffic and therefore travel with a negative wave speed. The maximum flow or capacity q_c occurs at critical density ρ_{cr}, while zero flow corresponds to the jam density ρ_j [34]. The passing rate r is the maximum rate at which the cumulative flow changes over a wave.

Combining the FD with Eq. (2-5) yields the LWR form of the conservation principle:

$$\frac{\partial \rho}{\partial t} + \frac{\partial Q(\rho)}{\partial s} = 0 \tag{2-7}$$

Given initial and boundary conditions the partial differential equation can be solved. Different boundary conditions generate different traffic states travelling at particular speeds. At some point, these states may cross one another. Yet, at one point there can only be one unique traffic state. In consequence, when the characteristics intersect a shockwave is formed where the wave speed can be determined using the following equation:

$$w_{21} = \frac{q_2 - q_1}{\rho_2 - \rho_1} \tag{2-8}$$

where q_1, q_2, ρ_1 and ρ_2 represent the flows and densities of the different traffic states, respectively. Models based on KWT represent vehicle propagation based on a FD of traffic flow. Furthermore, KWT can be used to determine the cumulative flow on the boundary of the link by following the path of the shockwave. Throughout this thesis, homogeneous signalized roads are considered, this means that the same FD holds for all locations.

2-2-2 Newell's simplified kinematic wave theory

Newell [35, 36, 37] presented the simplified kinematic wave theory where he simplifies the procedure of determining the cumulative flow. Newell uses KWT to directly evaluate the cumulative flow $N(s,t)$ for points in space-time instead of flows or densities. The conventional LWR-model can hence be rewritten where the cumulative flow is used as the new state variable:

$$\frac{\partial N(s,t)}{\partial t} - Q(\frac{-\partial N(s,t)}{\partial s}) = 0 \tag{2-9}$$

Newell's method uses a triangular shaped FD where there are only two characteristic wave speeds: v_f and w. According to Newell, the cumulative flow $N(s_P, t_P)$ can be calculated given a boundary $\mathcal{B}$ over which the cumulative flow $N_{\mathcal{B}}$ is known and from which a v_f-wave and a w-wave can be drawn to point P [38]. In this particular situation, the minimum of these two constraints yields N in point P. Figure 2-3 provides an illustration in which $N_{\mathcal{B}}$ is known over $\mathcal{B}$ and where N is estimated for point P. The constraining paths are obtained by drawing the characteristic wave speeds starting from $\mathcal{B}$. Then, the cumulative flow for point P can be estimated using:

$$N(s_P, t_P) = \min\left[N(s_0, t_2), N(s_L, t_1) + r \cdot (t_P - t_1)\right] \tag{2-10}$$

where s_0 is the location of the upstream link boundary, s_L is the location of the downstream link boundary, r is the passing rate and t_i is the time instant defined in Figure 2-3, $i = 1, 2, P$.

The considerable benefit of this simplified theory is that the cumulative flow for the full space-time domain can be estimated without following the precise path of the shockwave [34]. Without evaluation at intermediate times and locations, the solution for $N(s,t)$ can directly be determined from initial ($N(s,t_0)$) and boundary conditions ($N(s_0,t)$ and $N(s_L,t)$), which allows for an efficient and accurate procedure.

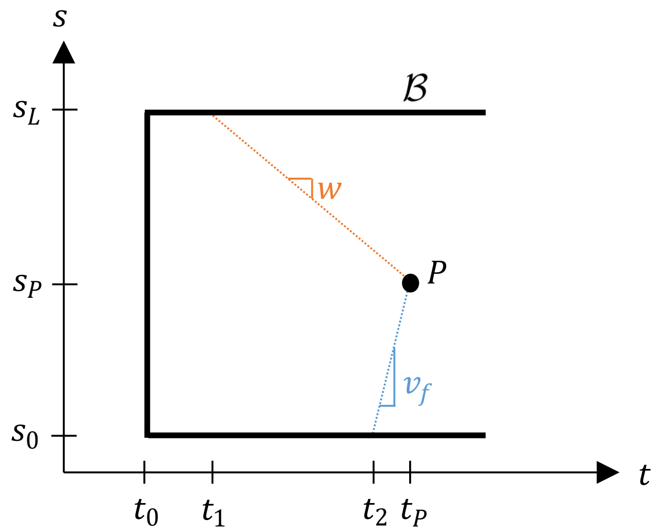

Figure 2-3: Estimation of the cumulative flow $N(s_P, t_P)$ using Newell's simplified method. The cumulative flow in point P can be determined by drawing a v_f-wave and a w-wave from the boundary $\mathcal{B}$ to P.

2-3 Queue and spillback effects on signalized roads

Most studies related to optimal speed trajectory control try to reduce idling time and smooth acceleration/deceleration maneuvers by only taking constraints induced by traffic signals into account. However, ignoring the spatial and temporal constraints by and to other road users could result in suboptimal or even infeasible solutions. Thus regarding surrounding traffic, there are two types of restrictions that are important to account for, i.e. queues and spillback.

2-3-1 Queue estimation

Queue estimation has already reached substantial research interest in many extensive studies about queue length estimation [39]. Especially accurate queue length estimation can help to improve speed trajectory control, which is important to reduce fuel consumption. Queue profile estimation has recently attracted research attention as such estimation is crucial for an extensive queue analysis. For example, at a signalized intersection, it can capture the spatiotemporal progression of the queue [40].

To facilitate real-time speed advice, control actions must be computed quickly [41]. As a result, tracking traffic densities in each road segment is unnecessary. However, to calculate the arrival time of the controlled vehicle accordingly, it is important to track the tail of the waiting queue. For example, the delay triangle is formed by the maximum speed v_M, minimum speed v_m and the red phase length of the traffic signal [42]. The advisory speed of the vehicle without considering the queue, denoted by v_0, is calculated by avoiding the delay triangle as demonstrated in Figure 2-4(a). However, the advisory speed with consideration of the queue, denoted by v_1, should be smaller than v_0 to prevent running into the queue as illustrated in Figure 2-4(b).

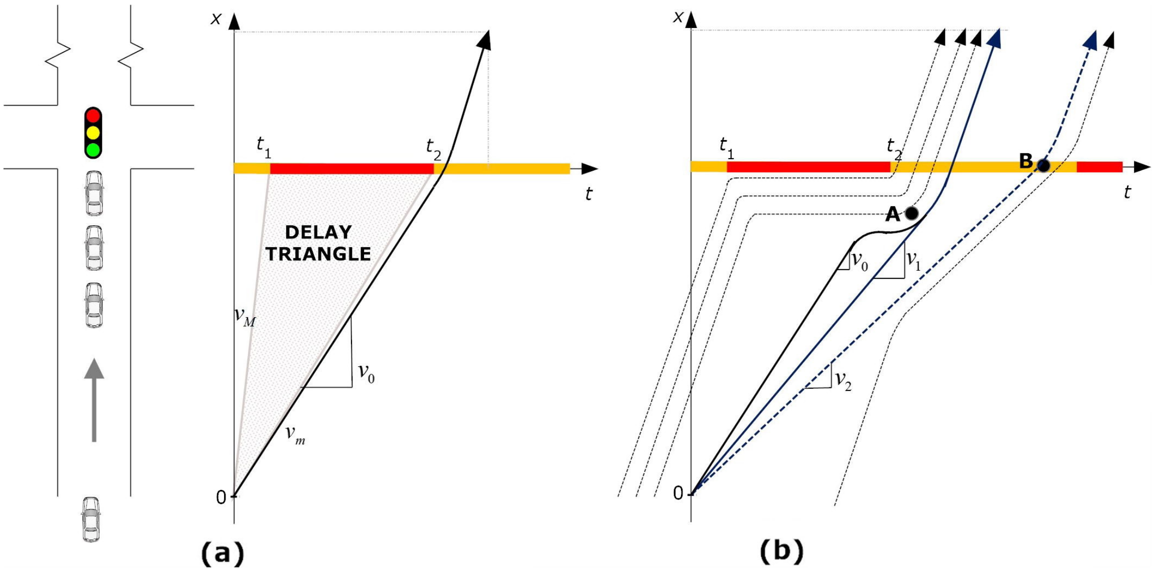

Figure 2-4: Optimal speed trajectory: (a) without considering the vehicle waiting queue, (b) with consideration of the vehicle waiting queue [18].

Some researchers assume that the controlled vehicle can acquire vehicle queue information accurately [43], however this may not always be possible in the future as not all vehicles can be connected [44]. Other studies utilize various queue prediction methods, including the Intelligent Driver Model [15], the LWR-model [27, 45] and the Shockwave Profile Model [46] to predict queue movement. As explained in Section 3-2-3, in this thesis queue propagation will be estimated by predicting the future cumulative flow curves, identifying the restrictive red periods and using KWT.

2-3-2 Vehicle spillback

Vehicle spillback remains a frequently observed phenomenon wherein a road cannot accommodate all inbound vehicles and the queue extends back [47]. There are two types of spillback, i.e. downstream and upstream spillback. Downstream spillback is caused by traffic signals. Consider a signalized road where several links are separated by traffic lights. If there is spillback on the most downstream link, then this will constrain the adjacent link. As a result, fewer vehicles can flow out even though the traffic signal is green. Downstream spillback can therefore also be regarded as an extension of the vehicle waiting queue and can be incorporated into queue estimation.

Upstream spillback is caused by vehicles. When implementing signalized intersections in optimal speed trajectory control, the main issue is how to deal with upstream spillback that is caused by the controlled vehicle but does not occur without control. Specifically, the controlled vehicle can create and worsen upstream spillback as a low cruise speed can disrupt other traffic and may lead to other upstream vehicles being unable to enter the link [25]. Hence, vehicle spillback represents a significant source of congestion and must be managed differently from queues that are limited to a single link [48, 49].

2-4 Speed trajectory control

Speed trajectory control gained recent research attention which is primarily due to the improvements in infrastructure-to-vehicle (I2V) communication and the standardization of signal phase and timing (SPaT) information [50]. Moreover, control methods have improved over time and have become more robust and complex, resulting in higher efficiency. Hence, research on mathematical algorithms to estimate fuel optimal speed profiles for vehicles driving on signalized roads have vastly been investigated in the literature. These approaches differ due to their difference in control approach, control requirements, type of vehicles, level of connectivity between the vehicles and level of autonomy of the vehicles regarded in the problem [51].

2-4-1 Model predictive control

MPC is a model-based control method that utilizes a dynamic model to predict system behavior and repeatedly calculate the optimal control sequence online in a receding horizon way. As shown in Figure 2-5, the receding horizon principle indicates an optimization problem is solved over a finite prediction horizon P at each control step k and only the first input of the optimal control sequence is implemented [22]. After which, the horizon is shifted by one time step and the optimization is restarted with new information about the measurements retrieved from the system. Thus, when a prediction model is available, an optimal control problem can be formulated that minimizes the objective function under the system dynamics and constraints. Hence, a general formulation of the optimization problem can be expressed as follows:

$$\min_{\boldsymbol{u}} \quad \mathcal{J} = \sum_{k=0}^{P-1} \ell(x(k), u(k)) + V_{\mathrm{f}}(x(P)) \tag{2-11a}$$

$$\text{subject to} \quad x(0) = x_0 \tag{2-11b}$$

$$x(k+1) = f(x(k), u(k)), \quad \forall k = 0, \ldots, P-1 \tag{2-11c}$$

$$(x(k), u(k)) \in \mathbb{Z}, \quad \forall k = 0, \ldots, P-1 \tag{2-11d}$$

$$x(P) \in \mathbb{X}_{\mathrm{f}} \tag{2-11e}$$

where P is the prediction horizon, x_0 is the current measured state, $\mathbb{Z}$ is the state and input constraints set, $\mathbb{X}_{\mathrm{f}}$ is the terminal constraint set and $\mathcal{J}$ is the cost. The cost function consists of two parts, the first term $\ell(\cdot)$ represents the cost of each stage k and the second term $V_{\mathrm{f}}(\cdot)$ represents the cost of the terminal state.

MPC represents a promising method for speed trajectory control of vehicles in urban areas since it can optimize over a combination of objectives, e.g. fuel consumption levels, emission rates, control effort and travel time of the individual vehicles. Because of the receding horizon approach, the latest system measurements are fed back to the controller closing the control loop, which makes MPC robust against uncertainties of the process. These uncertainties can be caused by model mismatches in the prediction model, environmental disturbances and

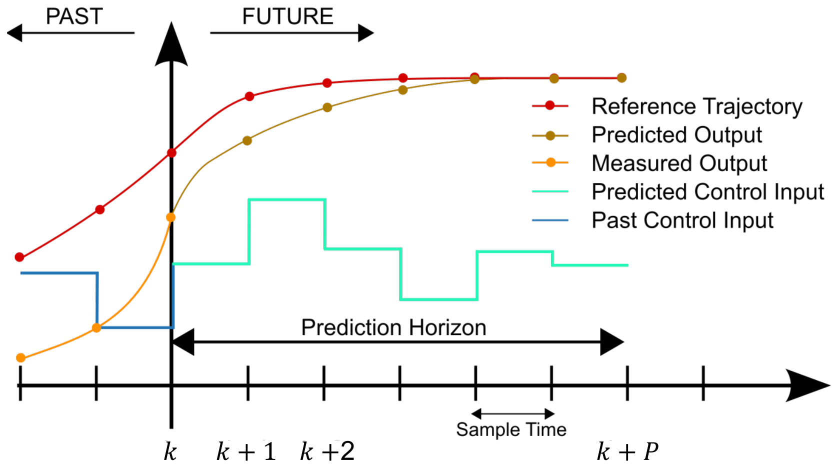

Figure 2-5: Receding horizon principle used in MPC. At each control step k the sequence of optimal control inputs is determined over the prediction horizon P. Only the first optimal control input is implemented and the horizon is shifted by one time step [52].

state estimation error. In addition, traffic imposed restrictions, e.g. traffic lights, speed limits, safe distance separation, queues and spillback, can be included as MPC can take state and input constraints into account. Another benefit of MPC is its modular design, allowing one to select and substitute the prediction model based on the trade-off between computational efficiency and accuracy or the control objectives [52].

Nevertheless, methods that use a finite prediction horizon make the optimization results mainly dependent on the horizon length. While a long prediction horizon with reliable data may result in better performance, it simultaneously requires a considerably longer computation time. Thus, for real-time computations, a short prediction horizon is preferred. However, a short horizon typically generates a speed trajectory less optimized for an entire route or the long-term [53]. Hence, the main challenge for MPC is to achieve adequate long-term optimization results with a computation time that is fast enough for real-time implementation.

Chapter 3

System model and problem formulation

Urban eco-driving attracted research attention due to the standardization of signal phase and timing (SPaT) information and the advancements in infrastructure-to-vehicle (I2V) communication [50]. Unlike traffic flow on highways, traffic on signalized roads is dominated by external events such as traffic signals. Vehicles come to a complete standstill before the stop line during the red phase of the traffic signal, producing shockwaves within the traffic stream. These shockwaves lead to vehicle acceleration/deceleration maneuvers and idling events, which increases fuel consumption [12]. Eco-driving studies, therefore, focus on intersection crossing where they utilize mathematical algorithms to compute fuel and traffic optimal speed profiles.

This chapter describes the vehicle control system, including the prediction model, the problem formulation and the operational and technological assumptions to make the problem feasible. To this extent, the vehicle model is introduced in Section 3-1 and the optimization objectives, constraints and optimal control problem are detailed in Section 3-2.

3-1 Vehicle model

The lateral movement of a vehicle within a single-lane is restricted by the road geometry. The responsibility of steering control of a vehicle for lane-keeping is therefore presumed to be handled perfectly by the driver. Hence, to improve fuel consumption, only the longitudinal dynamics of the vehicle need to be controlled. Generally, the state equation of a nonlinear control system at instant t can be expressed as:

$$\dot{x}(t) = f(x(t), u(t)) \tag{3-1}$$

where $x \in \mathbb{R}^{N_x}$ and $u \in \mathbb{R}^{N_u}$ are the state and input vector, respectively. For an individual vehicle entering the link, the state vector $x(t)$ of size $N_x = 2$ is defined as:

$$x(t) = [s(t), v(t)]^\top \tag{3-2}$$

where $s(t)$ and $v(t)$ are the position and speed of the controlled vehicle at time t, respectively. The relationships between the vehicle's position $s(t)$, speed $v(t)$ and acceleration $a(t)$ is represented by simple double integrator:

$$\dot{s}(t) = v(t) \tag{3-3a}$$
$$\dot{v}(t) = a(t) \tag{3-3b}$$

These differential equations define the vehicle dynamics in Eq. (3-1) as:

$$\dot{x}(t) = f(x(t), u(t)) = \begin{bmatrix} \dot{s}(t) \\ \dot{v}(t) \end{bmatrix} = \begin{bmatrix} v(t) \\ a(t) \end{bmatrix} \tag{3-4}$$

where the control input $u(t) \in \mathbb{R}^1$ is the acceleration rate at time t, i.e.

$$u(t) = a(t) \tag{3-5}$$

The vehicle acceleration rate at time t is dependent on the forces acting on the vehicle and is formulated as:

$$a(t) = \frac{F(t) - R(t)}{m} \tag{3-6}$$

where $F(t)$ is the driving force, $R(t)$ is the resistance force and m is the mass of the vehicle. The equations for the driving and resistance force are given by:

$$F(t) = mu(t) \tag{3-7a}$$
$$R(t) = \frac{\rho}{25.92} C_D C_h A_f v(t)^2 + gm\frac{C_r}{1000}\left(c_1 v(t) + c_2\right) + mgG(t) \tag{3-7b}$$

where ρ is the air density at sea level, C_D is the vehicle drag coefficient, C_h is a correction factor for the altitude and is calculated as $1 - 0.085H$ where H is the altitude in km, A_f is the frontal area of the vehicle, g is the gravitational acceleration, $G(t)$ is the roadway grade at time t and C_r, c_1 and c_2 are rolling resistance constants that vary as a function of the road surface, road condition and vehicle tire type.

Consequently, the state equation in (3-4) can be rewritten as follows where the time dependency is dropped:

$$f(x, u) = \begin{bmatrix} v \\ -\frac{1}{25.92m}\rho C_D C_h A_f v^2 - g\frac{C_r}{1000}(c_1 v + c_2) - gG + u \end{bmatrix} \tag{3-8}$$

3-2 Problem formulation

Existing eco-driving strategies vary with regard to their control method, level of connectivity between the vehicles, optimization objectives and constraints. The formulated optimization problems utilized in various studies minimize different objectives like fuel consumption, power consumption, emissions, travel time, control effort or a combination of these. Furthermore, with the developments in communication between road infrastructure and vehicles, it is possible to acquire real-time traffic SPaT information such that the probability of passing a green light is maximized [54]. Along with the traffic light constraint, other constraints can be integrated into the optimization framework to account for the legal speed limit, passenger comfort, safety and the surrounding traffic.

3-2-1 Objective function

Given the energy-oriented nature of this thesis, a logical choice would be to utilize a fuel consumption model as the cost of the algorithm. Nevertheless, the use of fuel consumption models within eco-driving studies is twofold. The fuel consumption model is explicitly integrated into the objective function of the optimal control problem [18] or is employed after the estimation of the fuel-optimal speed profile to determine the savings [54]. For those methods utilizing a fuel consumption model in their cost function, fuel optimal calculations are performed simultaneously with the computation of the optimal speed profile. While for the other approach, the speed trajectories obtained from simulation tools are provided to the fuel consumption model to evaluate the benefits [50].

Moreover, travel efficiency is of considerable importance in the optimal control problem. Consider the situation in which a vehicle must traverse a certain distance. The vehicle starts by transitioning to the optimal speed and then cruise the remaining distance at that speed. Generally speaking, this is not a satisfying solution; drivers do not travel at 30 km/h on an arterial road simply because it consumes the least amount of fuel. Most drivers prefer driving at the legal speed limit if the traffic conditions allow it. One could argue that implementing a lower speed bound would be a solution. However, if the vehicle begins with a lower speed than this bound, the optimization problem becomes infeasible. Using a speed restriction on the final state does not solve the issue either; the vehicle will simply cruise at the optimal speed before accelerating [55]. One option is to penalize the travel time with a parameter. The parameter represents a time penalty on the system added to the objective function. Without a specified travel time, it is calculated such that a specific speed, that minimizes fuel and time combined, equals the desired value [21]. Another solution is to augment the cost function by incorporating the vehicle's desired speed tracking. The appended term tries to minimize the deviation from the desired speed, typically chosen as the legal speed limit [17].

With the considerations above, the goal of the MPC controller is to improve fuel efficiency for vehicles proceeding through a signalized intersection while causing no adverse effect on travel efficiency. Hence, the cost function can be formulated as:

$$\min_{\boldsymbol{a}} \int_{t}^{t+T} \Big(\dot{m}_{\text{fuel}} \left(v(\tau), a(\tau) \right) + \left(v(\tau) - v_d \right)^2 \Big) \cdot d\tau \tag{3-9}$$

where t is the current time step, T is the prediction horizon over which the optimal control sequence is determined, $\dot{m}_{\text{fuel}}(\cdot)$ is the fuel consumption rate in l/s and v_d is the desired speed, set as 13.9 m/s.

Existing fuel consumption models are primarily functions of speed and acceleration (i.e. vehicle-based), but they are non-convex when considering fuel consumption while idling. This results in a non-convex function for the fuel consumption rate. By incorporating the vehicle's acceleration, the cost becomes convex for positive speeds [56]. For this reason, the weighted sum of the fuel consumption rate, the vehicle's desired speed tracking and the vehicle's acceleration is minimized. Consequently, the objective function can be reformulated as:

$$\min_{\boldsymbol{a}} \int_{t}^{t+T} \left(w_1 \dot{m}_{\text{fuel}} \left(v(\tau), a(\tau) \right) + w_2 (v(\tau) - v_{\text{d}})^2 + w_3 a(\tau)^2 \right) \cdot d\tau \tag{3-10}$$

where w_1, w_2 and w_3 are weighting terms providing a balance between fuel efficiency, travel efficiency and comfort, respectively. The importance of the chosen control objectives can vary depending on the traffic conditions, design decisions or individual vehicles. For example, some methods may prioritize safe driving, while others lay emphasis on mobility, accepting smaller spacings and higher risks.

Fuel consumption model

Many papers in the literature approximate the rate of fuel consumption as a function of the vehicle's speed and acceleration because obtaining an exact closed-form expression for fuel consumption is very complex [17]. Furthermore, in the majority of the strategies, the optimal control will be characterized by bang-bang control, in which the vehicle alternates between periods of maximum acceleration and gliding with the engine turned off [57]. Implementing the bang-bang solution in real-life is unrealistic because it is both uncomfortable for the driver and potentially disruptive to other vehicles in the network. To ensure that the system does not produce bang-bang control inputs, a second-order model with a positive second-order parameter is recommended [58]. Consequently, a second-order vehicle-based black-box fuel consumption model is selected to evaluate the energy implications of the controller as it provides a good compromise between model simplicity, applicability and accuracy.

The Virginia Tech Comprehensive Power-based Fuel Model (VT-CPFM) is frequently used in the literature because of its accuracy, simplicity and easy calibration [58]. The type 1 vehicle model of the VT-CPFM is a second-order vehicle-based black-box fuel consumption model and is formulated as follows:

$$\dot{m}_{\text{fuel}} \left(v(t), a(t) \right) = \begin{cases} \alpha_0 + \alpha_1 P(t) + \alpha_2 P(t)^2 & P(t) \geq 0 \\ \alpha_0 & P(t) < 0 \end{cases} \tag{3-11}$$

where α_0, α_1 and α_2 are the vehicle-specific model coefficients that need to be calibrated and $P(t)$ is the vehicle power in kW. The power exerted by the vehicle driveline at instant t is given by:

$$P(t) = \frac{R(t) + 1.04 m a(t)}{3600 \eta_d} \cdot v(t) \tag{3-12}$$

where $R(t)$ is the resistance force on the vehicle given by Eq. (3-7b) and η_d is the driveline efficiency.

3-2-2 Vehicle constraints

The aforementioned objective function (Eq. (3-10)) has the following vehicle constraints when solving for the optimal speed profile.

Vehicle dynamics constraint The longitudinal dynamics of the vehicle should obey the laws of physics, which are defined in Eq. (3-8).

Speed constraint For the consideration of feasibility and mobility, the speed constraint can be expressed as:

$$0 \leq v(t) \leq v_{\max} \tag{3-13}$$

where $v_{\max}$ is the maximum allowed speed, which is usually chosen as the legal speed limit. In this thesis, the speed limit is considered to be 13.9 m/s.

Acceleration constraint To ensure all acceleration solutions are feasible, the acceleration can be limited to the maximum value provided by the engine power and the deceleration can be limited by the braking conditions:

$$a_{\min} \leq a(t) \leq a_{\max} \tag{3-14}$$

The quantities $a_{\min}$ and $a_{\max}$ denote the maximum deceleration rate (negative value) and maximum acceleration rate, respectively. In this thesis, the AASHTO-recommended maximal deceleration rate of -3.4 m/s^2 is implemented (which is a comfortable deceleration for most drivers). Moreover, such decelerations are within the ability of the driver to maintain steering control and stay within the lane while braking on wet surfaces [59]. The maximal acceleration rate is assumed to be 3 m/s^2, which is a conservative estimate of a standard passenger car's maximum acceleration capability [12, 17].

3-2-3 Constraints imposed by traffic

In addition to the vehicle constraints, relevant traffic imposed restrictions should be included when solving for the optimal speed profile. These traffic constraints comprise downstream supply-related restrictions from traffic signals and other road users. This includes queues and the green periods that are available for the controlled vehicle.

To achieve this, it is assumed that necessary information about the status of the traffic signal can be obtained via wireless I2V communication. It is also assumed there is perfect downstream and upstream passing data till the current time. This data can be collected using induction loop detectors located at the upstream and downstream link boundaries.

This way, all inflowing and outflowing vehicles are observed and the cumulative flow curves at the boundaries till the current time are known. These curves are shared in real-time with the controlled vehicle when it drives on the link. In this manner, the controlled vehicle also knows its cumulative flow value.

The future downstream and upstream cumulative flow curves can be estimated using Newell's simplified method [34]. In theory, the MPC controller should not change these curves as this would mean the travel time of the controlled vehicle is increased and/or it causes upstream spillback that would not have occurred without control. Thereafter, the downstream restrictions can be determined based on the future cumulative flow curves, the LWR-model and the cumulative flow value of the controlled vehicle.

To begin with, the sampling time Δt, time instant the signal turns green t_g, time instant the signal turns red t_r, upstream segment L, upper bound restriction of the cumulative flow $\hat{N}_{\text{ub}}$, lower bound restriction of the cumulative flow $\hat{N}_{\text{lb}}$ and cumulative flow value of the controlled vehicle N_{cv} are initialized. Subsequently, a demand and an indicator function are defined. The demand is specified as the number of vehicles that want to enter the upstream link boundary between the current time t and the next time step $t + \Delta t$ [60]. Hence, the demand function equals:

$$D(t) = \int_{t}^{t+\Delta t} q_d(\tau) \cdot d\tau \tag{3-15}$$

where $q_d(\tau)$ is the demand flow.

An indicator is defined associated with the status of the traffic signal between the current time t and the next time step $t + \Delta t$. Hence, the indicator function equals:

$$I_{\text{color}}(t) = \begin{cases} 0, & \text{If the traffic light is red} \\ 1, & \text{If the traffic light is green} \end{cases} \tag{3-16}$$

Then, to include the restrictions several steps should be taken:

Step 1: Retrieve the current cumulative flow values

Retrieve the current cumulative flow values from the induction loop detectors located at the upstream and downstream link boundaries, i.e. $N(s_0, t)$ and $N(s_L, t)$ respectively.

Step 2: Estimate the future downstream and upstream cumulative flow curves

With the cumulative flow values from Step 1, the traffic signal information and future inflow information, one can estimate the future downstream and upstream cumulative flow curves over the entire prediction horizon T.

The upper bound restriction of the cumulative flow at the downstream link boundary is obtained by drawing a v_f-wave from the upstream boundary to the downstream boundary, as shown in Figure 3-1a. If a free-flow traffic state is observed at the downstream boundary at time $t + \Delta t$, then this state must have been emitted from the upstream boundary L/v_f

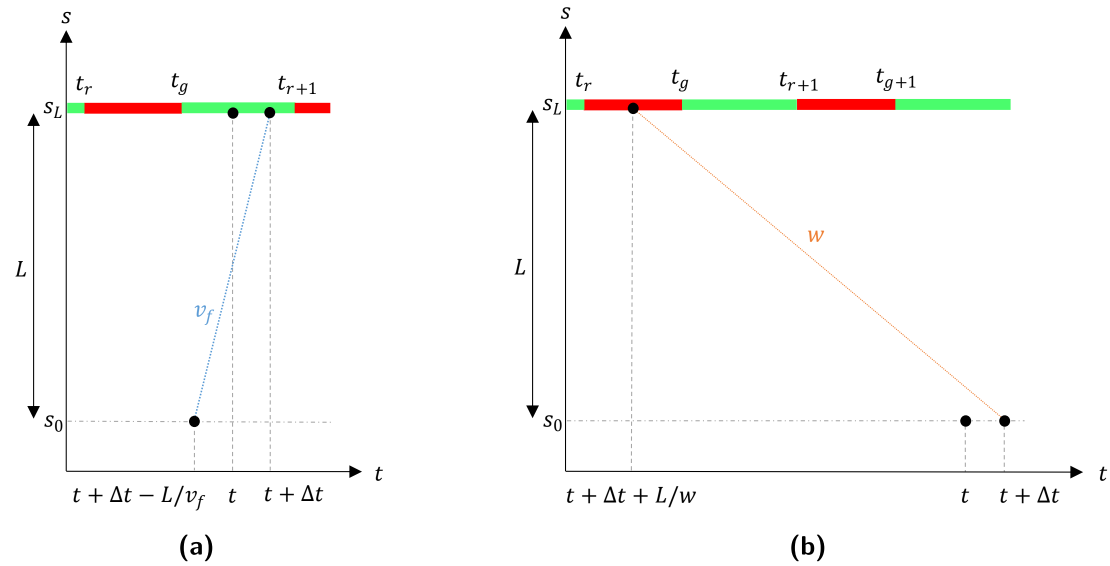

Figure 3-1: Propagation of a traffic state: (a) free-flow, (b) congested.

time units earlier. Therefore, the traffic conditions at $(s_L, t+\Delta t)$ and $(s_0, t+\Delta t - L/v_f)$ are identical. The cumulative flow difference between these two points is zero. This means that the cumulative flow at the downstream link end is a translation of the cumulative flow at the upstream boundary over L/v_f time units. As a result, the upper bound restriction at the downstream boundary equals:

$$\hat{N}_{\text{ub}}(s_L, t+\Delta t) = N(s_0, t+\Delta t - L/v_f) \tag{3-17}$$

The above-mentioned translation states that no vehicle can leave the link downstream until L/v_f time units have passed since entering the link upstream, i.e. the minimal link travel time must be respected.

The lower bound restriction of the cumulative flow at the downstream link boundary is obtained by determining the intersection outflow. If the signal is red, no vehicles can traverse the intersection and the discharge rate is zero. If the signal is green, vehicles can proceed through the intersection and the discharge rate is at capacity q_c. This means that the intersection outflow is related to the traffic signal status defined by Eq. (3-16). Consequently, the lower bound restriction at the downstream boundary can be formulated as:

$$\hat{N}_{\text{lb}}(s_L, t+\Delta t) = N(s_L, t) + q_c \cdot I_{\text{color}}(t) \cdot \Delta t \tag{3-18}$$

The number of vehicles that can cross the intersection is either constrained by Eq. (3-17) or Eq. (3-18). Consequently, the downstream cumulative flow is the flow taking into account these constraints. This is formulated as:

$$\hat{N}(s_L, t+\Delta t) = \min\left[\hat{N}_{\text{ub}}(s_L, t+\Delta t), \hat{N}_{\text{lb}}(s_L, t+\Delta t)\right] \tag{3-19}$$

The upper bound restriction of the cumulative flow at the upstream link boundary is obtained by determining the vehicle inflow. The vehicle inflow is related to the demand defined by Eq. (3-15). Consequently, the upper bound restriction at the upstream boundary can be formulated as:

$$\hat{N}_{\text{ub}}(s_0, t + \Delta t) = N(s_0, t) + D(t) \tag{3-20}$$

The lower bound restriction of the cumulative flow at the upstream link boundary is obtained by drawing a w-wave from the downstream boundary to the upstream boundary, as shown in Figure 3-1b. If a congested traffic state is observed at the upstream boundary at time $t + \Delta t$, then this state must have been emitted from the downstream boundary $-L/w$ time units earlier. Therefore, the traffic conditions at $(s_0, t + \Delta t)$ and $(s_L, t + \Delta t + L/w)$ are identical. The cumulative flow difference between these two points is the jam density times the length of the upstream segment, i.e. $\rho_j L$. This means that the cumulative flow at the upstream link end is a translation of the cumulative flow at the downstream boundary over $-L/w$ time units and $\rho_j L$ vehicle units. As a result, the lower bound restriction at the upstream boundary equals:

$$\hat{N}_{\text{lb}}(s_0, t + \Delta t) = N(s_L, t + \Delta t + L/w) + \rho_j L \tag{3-21}$$

The above-mentioned translation states that no vehicle can enter the link upstream until $-L/w$ time units have passed since the $(\rho_j L)^{th}$ vehicle has left the link downstream, i.e. an inflow restriction is induced due to downstream spillback.

The number of vehicles that can enter the link is either constrained by Eq. (3-21) or Eq. (3-20). Consequently, the upstream cumulative flow is the flow taking into account these constraints. This is formulated as:

$$\hat{N}(s_0, t + \Delta t) = \min\left[\hat{N}_{\text{ub}}(s_0, t + \Delta t), \hat{N}_{\text{lb}}(s_0, t + \Delta t)\right] \tag{3-22}$$

Step 3: Identify the restrictive red periods

With the estimated cumulative flow curves from Step 2 and the cumulative flow value of the controlled vehicle, one can identify the restrictive red periods.

For this purpose, the restrictive interval is divided into three times: t_{min}, t_{mid} and t_{max}. Here t_{min} represents the lower bound, t_{mid} represents an intermediate value and t_{max} represents the upper bound of the restrictive time interval. To find t_{min}, one should draw a backward propagating wave with speed w from the current position of the controlled vehicle (s, t) to the stop line of the intersection, as shown in Figure 3-2a. To find t_{mid}, one should draw a forward propagating wave with speed v_f from the current position of the controlled vehicle (s, t) to the stop line of the intersection, also shown in Figure 3-2a. Finally, with the estimated downstream cumulative flow curves, one knows when the controlled vehicle crosses the intersection and therefore the maximum time t_{max} that is restrictive. Subsequently, one can make a distinction between potentially and certainly restrictive red periods.

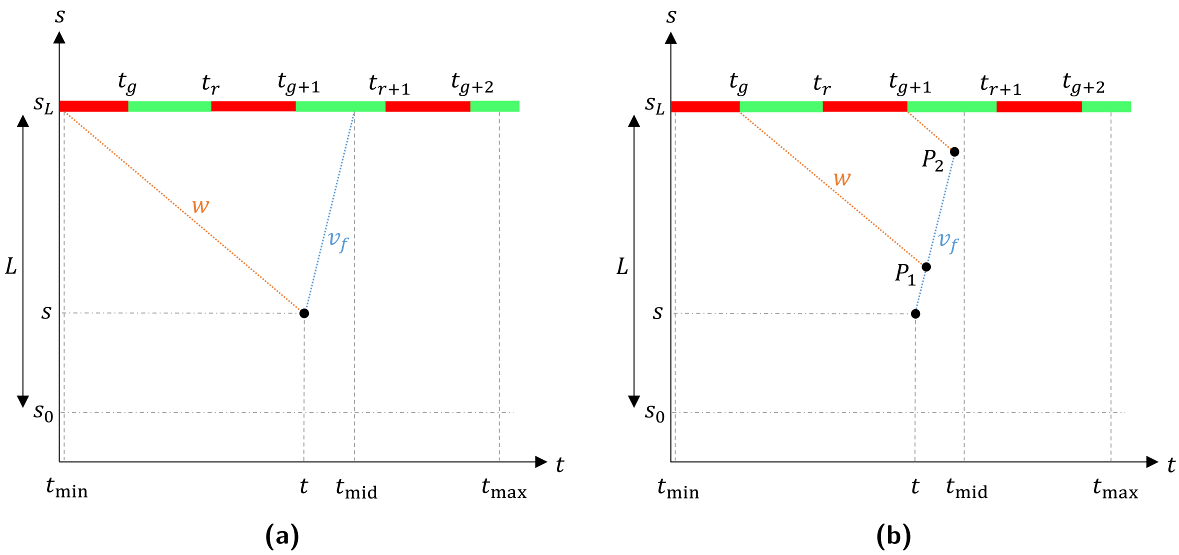

Figure 3-2: Identifying the restrictive red periods: (a) finding the restrictive time interval, (b) determining the potentially and certainly restrictive red periods.

Potentially restrictive red periods Each red period in the time interval $[t_{\min}, t_{\text{mid}}]$ is potentially restrictive. To determine which of the potential red periods causes a restriction, Newell's method is applied. Recall that Newell's simplified kinematic wave theory was defined as:

$$N(s_P, t_P) = \min\left[N(s_0, t_2), N(s_L, t_1) + r \cdot (t_P - t_1)\right] \tag{3-23}$$

where t_1 indicates the departing time of the w-wave, t_2 indicates the departing time of the v_f-wave and t_P indicates the time of point P.

This equation states that the cumulative flow in point P is either determined by the upstream boundary (first term on the right-hand side) or the downstream boundary (second term on the right-hand side). In this scenario, the first term on the right-hand side is the cumulative flow value of the controlled vehicle N_{cv}. The second term on the right-hand side indicates the maximum possible cumulative flow value at point P. Hence, the algorithm should check for each potential red period if the cumulative vehicle number of the controlled vehicle is smaller or equal to the maximum possible cumulative vehicle number. To illustrate, for point P_1 in Figure 3-2b this looks like:

$$N_{\text{cv}} \leq N(s_L, t_g) + r \cdot (t_{P_1} - t_g) \tag{3-24}$$

If the cumulative flow value of the controlled vehicle is bigger than the right-hand side of Eq. (3-24), that specific red period is restrictive and the algorithm has to consider a downstream constraint (Step 4).

Certainly restrictive red periods Each red period in the time interval $[t_{\text{mid}}, t_{\max}]$ is certainly restrictive. If the waiting queue does not completely dissolve by the end of the current cycle, a residual queue is formed. The residual queue causes an initial queue to occur at the start of

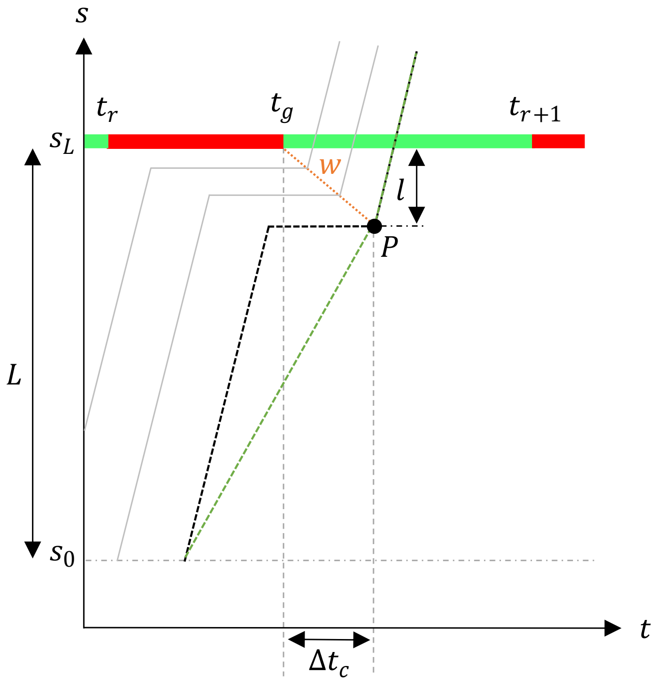

Figure 3-3: Trajectories of vehicles and the characteristic wave speed for the formulation of the downstream supply-related constraints. The dashed black line represents the trajectory without considering the queue and the dashed green line represents the trajectory considering the queue.

the next cycle, which must first clear before the controlled vehicle can cross the intersection. As a consequence, the next red period is certainly restrictive and the algorithm has to consider a downstream constraint (Step 4).

Step 4: Formulate the downstream supply-related constraints

For each restrictive red period found in Step 3, a point in the space-time domain is introduced. What follows is a general explanation of the equations to determine the position of that specific point and the formulation of the downstream constraint.

As shown in Figure 3-3, point P represents the spatial and temporal constraint imposed by the presence of the vehicle queue on the signalized road. The queue dissipation time and location can be calculated with the following formulas:

$$\Delta t_c = \frac{N_{\text{cv}} - N(s_L, t_g)}{r} \tag{3-25a}$$

$$l = w \cdot \Delta t_c \tag{3-25b}$$

The downstream restriction is designed to prevent the controlled vehicle from idling in the queue. The position of point P indicates the queue would reach its maximum length at time $t_g + \Delta t_c$, which is located at $L - l$. Hence, this constraint essentially aims to assure the position of the controlled vehicle at the dissipation time of the queue is not beyond the tail location of the queue. Consequently, the following downstream supply-related constraint is formulated for each restrictive red period:

$$s(t_g + \Delta t_c) \leq L - l \tag{3-26}$$

3-2-4 Minimum-fuel control problem

The minimum fuel consumption problem is expressed as an optimal control problem. By solving this problem, the control inputs are obtained that minimize the amount of fuel consumed. It is assumed the calculated optimal control input can be fed directly to the controlled vehicle via an advanced cruise control system capable of operating in stop-and-go traffic. With the foregoing considerations, a general formulation of the optimal control problem can be cast as follows. Subject to the system dynamics and constraints in Eqs. (3-1)-(3-26), minimize the cost function in (3-10) at each time t with the current measured state $x(t)$ used as the initial condition.

Note that, the solution to the optimal control problem may be suboptimal as the MPC controller does not use a multi-start algorithm. A multi-start algorithm should have been used as the prediction model of the controller is highly nonlinear and the optimization problem, therefore, becomes non-convex. With a multi-start algorithm, the same optimization problem is solved multiple times using a different set of initial conditions. This way, the chance of finding a global solution instead of a local solution increases.

Chapter 4

Simulation case studies and results

The effectiveness of the predictive speed control (PSC) strategy will be evaluated using simulations. The simulations will be executed in Simulation of Urban MObility (SUMO) [61]. SUMO is a widely used open source microscopic traffic simulator for modelling and simulating urban traffic networks. To communicate between SUMO and MATLAB, the TraCI [62] interface is used. By connecting SUMO and MATLAB the user can: (i) access, modify and manipulate the traffic network developed in SUMO from MATLAB; (ii) control the dynamics and movements of the vehicles and navigate them in the traffic network from MATLAB; (iii) control the traffic actuators from MATLAB; (iv) evaluate, assess, improve and simulate the performance of the developed control system.

In this chapter, five case studies are conducted based on the simulation set-up in Section 4-1. The benchmark algorithm to evaluate the performance of the Eco-PSC algorithm is explained in Section 4-2. Then, three case studies are performed in various traffic conditions to assess the benefits of the proposed algorithm. Finally, two case studies are executed to investigate the impact of market penetration rates and stochasticity in traffic behavior on the algorithm performance.

4-1 Simulation set-up

The network that will be considered in the simulation case studies is shown in Figure 4-1. A small network is taken into consideration which consists of a single-lane road with one signalized intersection. The control zone includes both the upstream segment $L = 400$ meters and the downstream segment $d = 200$ meters, since ignoring acceleration behavior after queue dissipation results in more fuel usage when the vehicle traverses the intersection. The length of the vehicles regarded in the case studies is 5 meters.

The lane that is connected to the traffic signal will receive green light signals in alternating phases, such that the vehicles may pass the junction. For the signal phase and timing (SPaT)

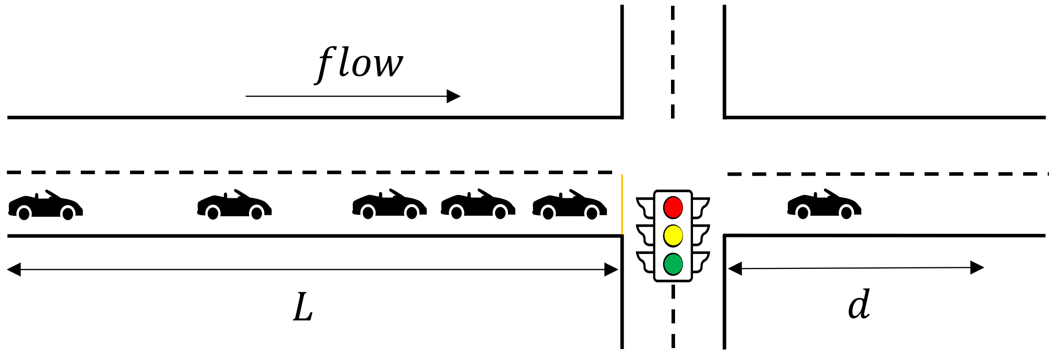

Figure 4-1: Configuration of the signalized intersection considered in the simulations. The control zone includes both the upstream and downstream segments L and d, respectively.

plan the duration of the green and red indicators are 30 seconds each. It is assumed that necessary information about the status of the traffic signal can be accessed through infrastructure-to-vehicle (I2V) communication. Furthermore, induction loop detectors are located at the upstream and downstream link boundaries. This way, all inflowing and outflowing vehicles are observed and the cumulative flow curves at the boundaries till the current time are known. These curves are shared in real-time with the controlled vehicle when it drives on the link. In such manner, the controlled vehicle also knows its cumulative flow value.

Finally, a suitable prediction horizon of $T = 90$ seconds is chosen to cover the prediction of the future cumulative flow curves in various traffic conditions. The control horizon is chosen to be equal to the prediction horizon. The controlled vehicle receives advisory speeds from the algorithm, which are updated every second.

4-1-1 Parameter identification

In this subsection, the weights used for fuel efficiency, travel efficiency and comfort, the input parameters to calibrate the VT-CPFM fuel consumption model and the fundamental diagram (FD) parameters to calibrate the Eco-PSC algorithm are given.

Weighting terms

In Eq. (3-10), the weights w_1, w_2 and w_3 balance the effects of the fuel consumption, speed deviation and control effort term. A high w_1 value emphasizes fuel consumption and produces a speed trajectory with a low speed and a long travel time, which is unsuitable for actual driving because it obstructs traffic. A large value of w_2 results in a speed trajectory with sharp accelerations/decelerations to the desired speed and a short travel time, which is also not recommended due to its high fuel consumption rate. Lastly, the value of w_3 encourages minimal speed change, enhancing driving comfort. As a result, a good trade-off between fuel efficiency, travel efficiency and comfort is necessary. In this thesis, the decision is made to emphasize on fuel consumption savings, accepting lower speeds and longer travel times. Furthermore, since passenger comfort is also incorporated in the acceleration constraint this is not prioritized. Hence, the following weights that are recommended by Hu et al. [63] are considered: $w_1 = 20$, $w_2 = 0.5$ and $w_3 = 1$.

Table 4-1: Parameters of the type 1 vehicle model of VT-CPFM.

Parameter	m [kg]	C_d [-]	C_h [-]	A_f [m^2]	ρ [kg/m^3]	g [m/s^2]	G(t) [deg]
Value	1453	0.30	1	2.32	1.23	9.81	0
Parameter	C_r [-]	c_1 [-]	c_2 [-]	η_d [-]	α_0 [-]	α_1 [-]	α_2 [-]
Value	1.75	0.03	4.58	0.92	5.92×10^{-4}	4.95×10^{-4}	1.00×10^{-6}

VT-CPFM parameters

The vehicle under investigation is a 2010 Honda Accord, which can be modeled as a standard drive train, an internal combustion engine and a five-speed automated mechanical transmission. The values of the input parameters for the VT-CPFM model are given in Table 4-1. Subsequently, the VT-CPFM MATLAB calibration tool was used to calibrate the vehicle-specific model coefficients α_0, α_1 and α_2 [58]. It is assumed all vehicles in the network are the type 1 vehicle of the VT-CPFM model.

Fundamental diagram parameters

The triangular shaped FD is described by three parameters: a fixed free-flow speed v_f, the capacity q_c and the jam density ρ_j [34]. The free-flow speed is the speed of the vehicles at zero density and is set as $v_f = 50$ km/h. If the traffic signal is green, then the intersection outflow is at the rate of the capacity. The average driver's minimum time headway is approximately 1.5-1.8 seconds, so a typical capacity value of 2000 to 2400 veh/h is found [64]. For the jam density, an estimation can be made based on the length of the vehicles and the distance they keep at standstill. The length of the vehicles regarded in the simulations is 5 meters and at standstill the minimum spacing is approximately 2-3 meters, which means the jam density is 125 to 142 [28]. The capacity and jam density are important parameters that define the slope of the FD branches and therefore influence the wave speed and passing rate. The capacity and jam density influence on the algorithm performance is summarized in Table 4-2.

To choose a suitable combination of q_c and ρ_j, the computed optimal speed trajectory is compared to the actual speed trajectory of the controlled vehicle for different parameter combinations in Figure 4-2. From Table 4-2, we can observe that the least amount of fuel is consumed for the combination $q_c = 2250$ and $\rho_j = 125$. If we then compare the computed optimal speed trajectory with the actual speed profile in Figure 4-2a, we see a good fit between the two curves. However, this parameter combination significantly overestimates the queue. The second option, considering travel time, is the combination $q_c = 2400$ and $\rho_j = 142$. If we compare the calculated optimal speed trajectory with the actual speed profile in Figure 4-2b, we see that this parameter combination significantly underestimates the queue. A balanced trade-off between fuel consumption and travel time is provided by the combination $q_c = 2280$ and $\rho_j = 138$. This parameter combination offers an optimal fit between both speed profiles as depicted in Figure 4-2c. Therefore, in the simulations the capacity and jam density are set as $q_c = 2280$ veh/h and $\rho_j = 138$ veh/km.

Table 4-2: Influence of the parameters capacity and jam density on the algorithm performance.

	Fuel consumption [ml]	Travel time [s]
$q_c = 2400,\ \rho_j = 142$	67.32	57.00
$q_c = 2400,\ \rho_j = 133$	66.09	57.07
$q_c = 2400,\ \rho_j = 125$	65.42	57.17
$q_c = 2250,\ \rho_j = 142$	65.19	57.23
$q_c = 2250,\ \rho_j = 133$	65.07	57.51
$q_c = 2250,\ \rho_j = 125$	64.99	57.84
$q_c = 2117,\ \rho_j = 142$	65.75	58.19
$q_c = 2117,\ \rho_j = 133$	65.66	58.52
$q_c = 2117,\ \rho_j = 125$	65.57	58.85
$q_c = 2000,\ \rho_j = 142$	66.33	59.20
$q_c = 2000,\ \rho_j = 133$	66.26	59.53
$q_c = 2000,\ \rho_j = 125$	66.20	59.86

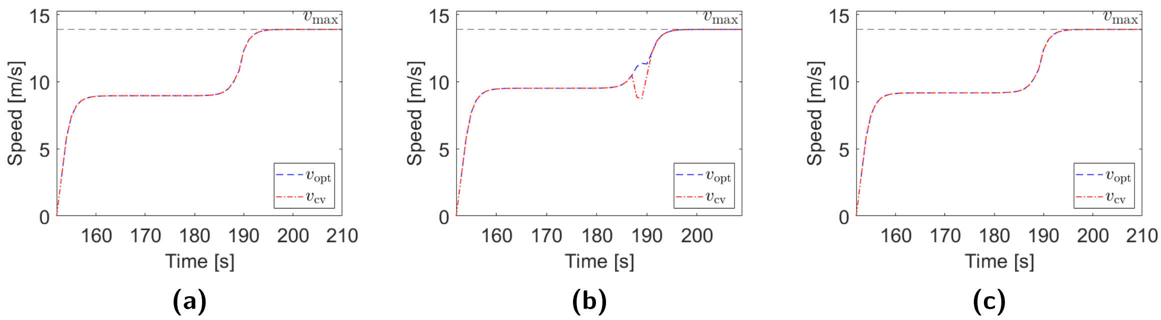

Figure 4-2: Speed profiles for different FD parameter combinations where v_{opt} is the computed optimal speed and v_{cv} is the actual speed of the controlled vehicle: (a) $q_c = 2250$ and $\rho_j = 125$, (b) $q_c = 2400$ and $\rho_j = 142$, (c) $q_c = 2280$ and $\rho_j = 138$.

4-1-2 Performance measures

The effectiveness of the Eco-PSC algorithm will be evaluated in terms of system performance and computational efficiency. The system performance will be measured by the fuel consumption (FC) and the travel time (TT) of the controlled vehicle. Besides these absolute values, the performance of the algorithm is also compared against a baseline policy. A cooperative adaptive cruise control (CACC) strategy based on eco-driving is chosen as the baseline policy. The relative change of the PSC strategy with respect to the CACC strategy will be used to benchmark the system performance. For instance, the relative change in fuel consumption $\mathrm{FC}_{\mathrm{rel}}$ is calculated by:

$$\mathrm{FC}_{\mathrm{rel}} = \frac{\mathrm{FC}_{\mathrm{PSC}} - \mathrm{FC}_{\mathrm{CACC}}}{\mathrm{FC}_{\mathrm{CACC}}} \cdot 100\% \tag{4-1}$$

Where $\mathrm{FC}_{(\cdot)}$ denotes the fuel consumption associated with the strategy $(\cdot)$.

In like manner, $\mathrm{TT}_{\mathrm{rel}}$ is defined for the relative change in travel time for the controlled vehicle:

$$\mathrm{TT}_{\mathrm{rel}} = \frac{\mathrm{TT}_{\mathrm{PSC}} - \mathrm{TT}_{\mathrm{CACC}}}{\mathrm{TT}_{\mathrm{CACC}}} \cdot 100\% \tag{4-2}$$

Here $\mathrm{TT}_{(\cdot)}$ denotes the travel time associated with the strategy $(\cdot)$.

Note that throughout the case studies, an increase in travel time will be observed. This can be explained by the choice of weighting terms used for fuel and travel efficiency. The decision was made to prioritize fuel efficiency, accepting longer travel times. In addition, the Eco-PSC algorithm slightly overestimates the tail location of the queue. This can be explained by the discretization error of the queue constraint. The sampling time determines the trade-off between accuracy and tractability. A shorter sampling time would reduce the discretization error but increase the computational burden.

Furthermore, to establish if the Eco-PSC algorithm is real-time implementable, the computation time of the MPC controller will be evaluated. The processor time of the online optimization step will be used to determine the computational efficiency. If the maximum processor time $\mathrm{CT}_{\mathrm{max}}$ of the online optimization step is less than the sampling interval of the system, the controller will be real-time implementable. The simulations are performed on an Intel(R) Core(TM) i7-8550U CPU @ 1.80GHz and 16GB RAM. The CPU computation time of the online optimization step is obtained using the CPU command in MATLAB.

4-1-3 Demand profiles

To evaluate the benefits of the Eco-PSC algorithm, different demand profiles are created with the route generator in SUMO, where routes are generated based on flow definitions. The first three cases, i.e. single queue, residual queue and upstream spillback, are developed to present scenarios for which undersaturated and oversaturated traffic conditions occur in the network. The demand profiles that have been used in case studies I, II and III are presented in Figure 4-3. Case study IV has been conducted with a constant demand flow of $q_d = 900$ veh/h. Lastly, Case study V has been performed with the demand profile of the single queue case and a constant demand flow of $q_d = 900$ veh/h.

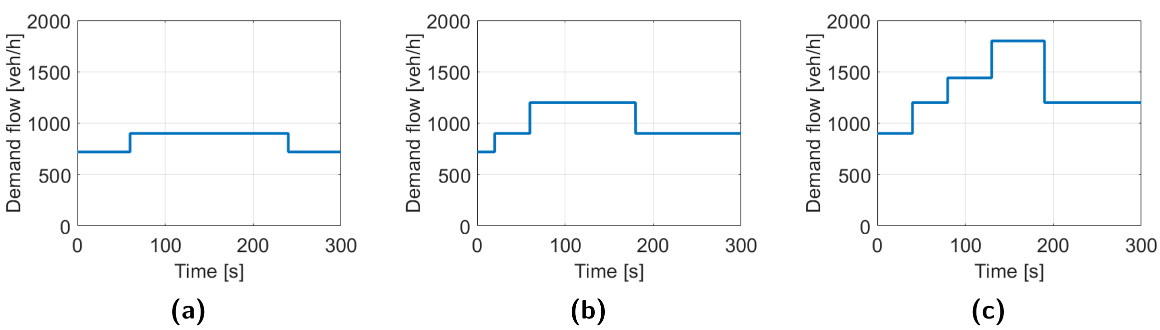

Figure 4-3: Demand profiles generated to simulate various traffic scenarios: (a) single queue case, (b) residual queue case, (c) upstream spillback case.

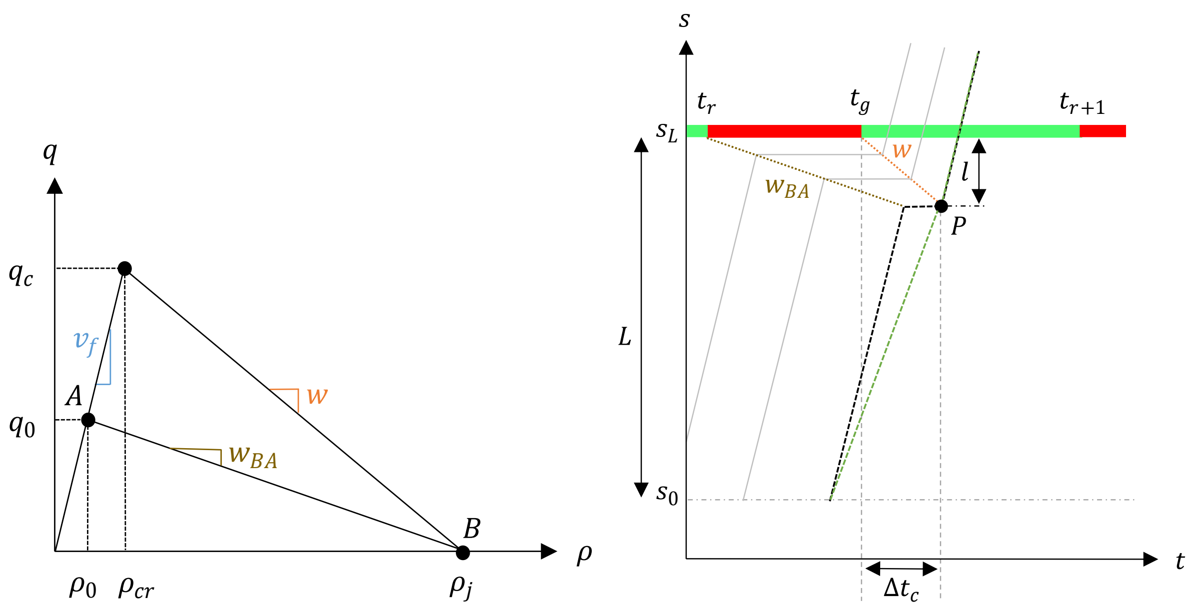

Figure 4-4: Traffic state dynamics at a signalized intersection: (a) fundamental diagram with important parameters and wave speeds, (b) trajectories of vehicles and shockwaves. The dashed black line represents the trajectory without consideration of the queue and the dashed green line represents the trajectory with consideration of the queue.

4-2 Benchmark algorithm

The Eco-CACC algorithm designed by Yang et al. [27] is chosen as the baseline strategy. The algorithm exploits SPaT information obtained via I2V communication and predicts vehicle queues to compute optimal speed profiles. In the algorithm, the length of the queue is estimated using the LWR-model and the dissipation time of the queue is estimated using SPaT information. What follows is a general explanation of the Eco-CACC algorithm.

Assume that the flow entering the intersection is q_0 and that the upstream traffic state is A, as shown in Figure 4-4a. If the traffic signal status is red, no vehicles can traverse the intersection and the upstream state becomes B. Subsequently, a queuing shockwave is generated that propagates backward with speed:

$$w_{BA} = \frac{q_0}{\rho_0 - \rho_j} \tag{4-3}$$

As soon as the light turns green, the intersection starts to release vehicles at the rate of the capacity q_c. As a result, a backward propagating wave is generated to discharge the queue upstream of the intersection, as illustrated in Figure 4-4b. The speed of the discharge shockwave is calculated as:

$$w = \frac{q_c}{\rho_{cr} - \rho_j} \tag{4-4}$$

At time t the controlled vehicle enters the control zone with speed v_0. Then, the queue length upstream of the intersection can be estimated using the following formula:

$$l = \begin{cases} \frac{w_{BA}}{v_f + w_{BA}}\left[L - v_f\left(t_r - t\right)\right], & \forall t \in \left[t_r - \frac{d}{v_f}, t_g + \frac{w_{BA}(t_g - t_r)}{w_{BA}+w}\right] \\ 0, & \text{Otherwise} \end{cases} \tag{4-5}$$

The objective of the Eco-CACC algorithm is to minimize the fuel consumption for vehicles proceeding though the signalized intersection. The mathematical formulation of the algorithm can be stated as:

$$\min_{a_1, a_2} \quad \int_{t_0}^{t_4} F(v(\tau))d\tau \tag{4-6a}$$

$$\text{subject to} \quad s(t_0) = s_0 \tag{4-6b}$$

$$s(t_4) = L + d \tag{4-6c}$$

$$a_{\min} \leq a_1 \leq a_{\max} \tag{4-6d}$$

$$0 \leq a_2 \leq a_{\max} \tag{4-6e}$$

$$v_c = v_0 + a_1(t_1 - t_0) \tag{4-6f}$$

$$v_0(t_1 - t_0) + \frac{1}{2}a_1(t_1 - t_0)^2 + v_c(t_2 - t_1) = L - l \tag{4-6g}$$

$$t_2 = t_g + \frac{l}{w} \tag{4-6h}$$

$$v_f = v_c + a_2(t_3 - t_2) \tag{4-6i}$$

$$v_c(t_3 - t_2) + \frac{1}{2}a_2(t_3 - t_2)^2 + v_f(t_4 - t_3) = d + l \tag{4-6j}$$

$$v(a_1, a_2, \tau) = \begin{cases} v_0 + a_1\left(\tau - t_0\right), & t_0 \leq \tau < t_1 \\ v_c, & t_1 \leq \tau < t_2 \\ v_c + a_2\left(\tau - t_2\right), & t_2 \leq \tau < t_3 \\ v_f, & t_3 \leq \tau \leq t_4 \end{cases} \tag{4-6k}$$

where $F(\cdot)$ is the fuel consumption rate computed using the VT-CPFM model (see Section 3-2-1), v_c is the cruise speed to the intersection and t_i is the time instant given the road traffic condition, $i = 0, 1, \ldots, 4$.

Eqs. (4-6f)-(4-6h) illustrate that the controlled vehicle accelerates to the cruise speed v_c and crosses the intersection when the queue is discharged. Eqs. (4-6i) and (4-6j) demonstrate that the controlled vehicle accelerates to the legal speed limit. Eq. (4-6k) indicates that given the traffic state, the speed profile is a function of the acceleration/deceleration rates, i.e. a_1 and a_2.

4-3 Case study I - single queue

In this section, the effectiveness of the Eco-PSC algorithm in undersaturated traffic conditions where queues can completely dissolve in a single cycle is evaluated. The demand profile of

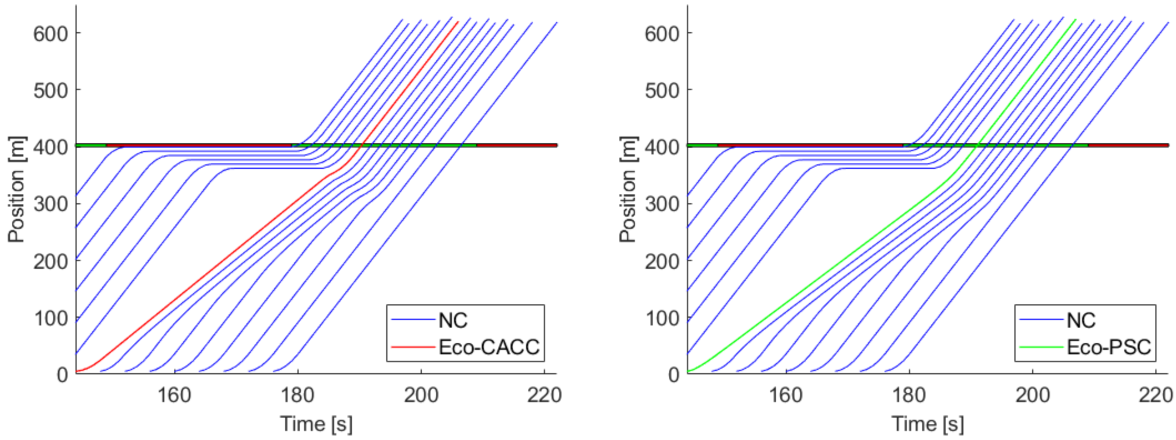

(a) **(b)**

Figure 4-5: Vehicle trajectories around the signalized intersection in Case study I: (a) the blue lines represent the non-controlled vehicles and the red line represents the CACC vehicle, (b) the blue lines represent the non-controlled vehicles and the green line represents the PSC vehicle.

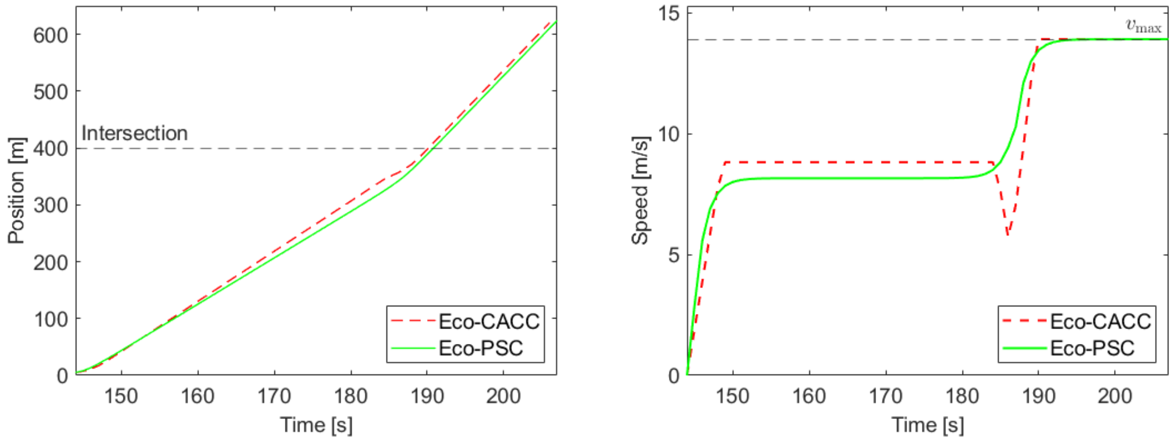

(a) **(b)**

Figure 4-6: Eco-driving in Case study I: (a) comparison of vehicle trajectories of the controlled vehicle, (b) comparison of speed profiles of the controlled vehicle.

Figure 4-3a is loaded to the intersection for 300 seconds and the controlled vehicle enters the network at $t = 144$ seconds.

Figure 4-5 illustrates the trajectories of all vehicles for the two eco-driving algorithms over one signal cycle, where the traffic light is located at 400 meters. Figure 4-5a shows the vehicle trajectories after applying the Eco-CACC algorithm. As can be seen in the figure, the controlled vehicle cruises towards the traffic signal and just catches the tail of the vehicle waiting queue. Because of the queue, the vehicle has to slow down and wait for the queue to be released before it can continue its path. While in Figure 4-5b, the Eco-PSC algorithm ensures that the vehicle can cruise towards the intersection and catch the tail of the queue when it is discharged. This way, the vehicle can avoid slowing down ahead of the traffic signal and precisely follow the calculated optimal trajectory.

Figure 4-6a compares the trajectories of the controlled vehicle for the two eco-driving algorithms. The trajectory computed by the Eco-PSC algorithm is smoother than the benchmark algorithm. This can be explained by the fact that the benchmark algorithm underestimates the tail location of the queue. A possible reason for this inaccurate estimation is that the queue length is predicted based on the FD, which was calibrated for the PSC method. Hence, with different values for the capacity and jam density, the performance of the benchmark algorithm could increase. Nevertheless, the travel time of the vehicle driving with the Eco-CACC algorithm is slightly shorter. Compared to the benchmark algorithm, the travel time of the PSC vehicle is increased by 1.14%. The increase in travel time is due to the choice of weighting terms and the discretization error. For a detailed explanation see Section 4-1-2.

Figure 4-6b compares the speed profiles of the controlled vehicle for the two eco-driving algorithms. The speed profile computed by the Eco-PSC algorithm is smoother than the benchmark algorithm. For the benchmark algorithm, the vehicle cruises at a speed of 8.82 m/s and the speed drops due to the underestimation of the queue for approximately 4 seconds. While being controlled by the Eco-PSC algorithm, the vehicle cruises at 8.15 m/s and does not crises its speed upstream of the intersection. Furthermore, the fuel consumption levels by the controlled vehicle are 71.24 ml for the benchmark algorithm and 68.14 ml for the Eco-PSC algorithm, see Table 4-3. Hence, the Eco-PSC algorithm is the more efficient control method, reducing the fuel consumption levels by 4.35%.

Besides the controlled vehicle, both algorithms smooth the trajectories of the non-controlled vehicles (as seen in Figure 4-5). Given that the non-controlled vehicles are driven by the Krauss car-following model [65] and thus follow the behavior of their leader. This means that the Eco-PSC algorithm can further minimize the overall fuel consumption around the intersection. The example above demonstrates that the algorithm reduces the average fuel consumption levels by 1.12% compared to the benchmark algorithm.

Lastly, it is crucial that the algorithm is simple in order to keep the optimization problem computationally tractable for real-time execution. SUMO facilitates an option for interactive online simulation and the proposed algorithm is found to be fast enough to run a vehicle without causing delays. A maximum computation time of 0.44 seconds per sampling interval was observed, as presented in Table 4-3.

Table 4-3: Performance evaluation of the Eco-PSC algorithm in terms of fuel consumption, travel time, maximum computation time and relative change in fuel consumption and travel time compared to the benchmark algorithm in Case study I. Furthermore, the average fuel consumption and travel time of the non-controlled vehicles related to the eco-driving strategies, denoted by $\mathrm{NC_{CACC}}$ and $\mathrm{NC_{PSC}}$, are also presented.

Control	FC [ml]	TT [s]	$\mathrm{FC_{rel}}$ [%]	$\mathrm{TT_{rel}}$ [%]	$\mathrm{CT_{max}}$ [s]
Eco-CACC	71.24	61.62	-	-	-
Eco-PSC	68.14	62.32	-4.35	+1.14	0.44
$\mathrm{NC_{CACC}}$	77.51	59.34	-	-	-
$\mathrm{NC_{PSC}}$	76.64	59.63	-1.12	+0.49	-

4-4 Case study II - residual queue

In this section, the effectiveness of the Eco-PSC algorithm in oversaturated traffic conditions where residual queues are formed is evaluated. However, in the design of the Eco-CACC algorithm, one critical assumption is that queues can dissolve in a single cycle. Hence, one drawback of the benchmark algorithm is that it fails to provide the optimal speed profile in oversaturated traffic conditions. To circumvent this problem, in case of an emergency, the acceleration range can be overruled by the autonomous emergency braking system to ensure safety. The emergency deceleration (i.e. the maximal physically possible deceleration for the vehicle) is equal to the default value of -9 m/s^2 [61]. Now, the demand profile of Figure 4-3b is loaded to the intersection for 300 seconds and the controlled vehicle enters the network at $t = 177$ seconds.

Figure 4-7 illustrates the trajectories of all vehicles for the two eco-driving algorithms over one and a half cycle length, where the traffic signal is located at 400 meters. Figure 4-7a shows the vehicle trajectories after implementing the Eco-CACC algorithm. As can be seen in the figure, the controlled vehicle predicts the tail location of the first queue and adapts its path. Then, the behavior of the vehicle is similar to the behavior without control. The vehicle just follows its leader and comes to a complete stop ahead of the traffic signal waiting for the green light to discharge the second queue. While in Figure 4-7b, the Eco-PSC algorithm ensures the vehicle can cruise towards the intersection and catch the tail of the second queue when it is released. This way, the vehicle can prevent coming to a complete stop upstream of the traffic signal and exactly follow the computed optimal trajectory.

Figure 4-8a compares the trajectories of the controlled vehicle for the two eco-driving algorithms. The trajectory computed by the Eco-PSC algorithm is much smoother than the benchmark algorithm. In this example, the Eco-CACC algorithm only estimates the tail location of the first queue. Because of residual queues, the algorithm cannot avoid incurring a complete stop, significantly reducing its benefits. Nevertheless, the travel time of the vehicle

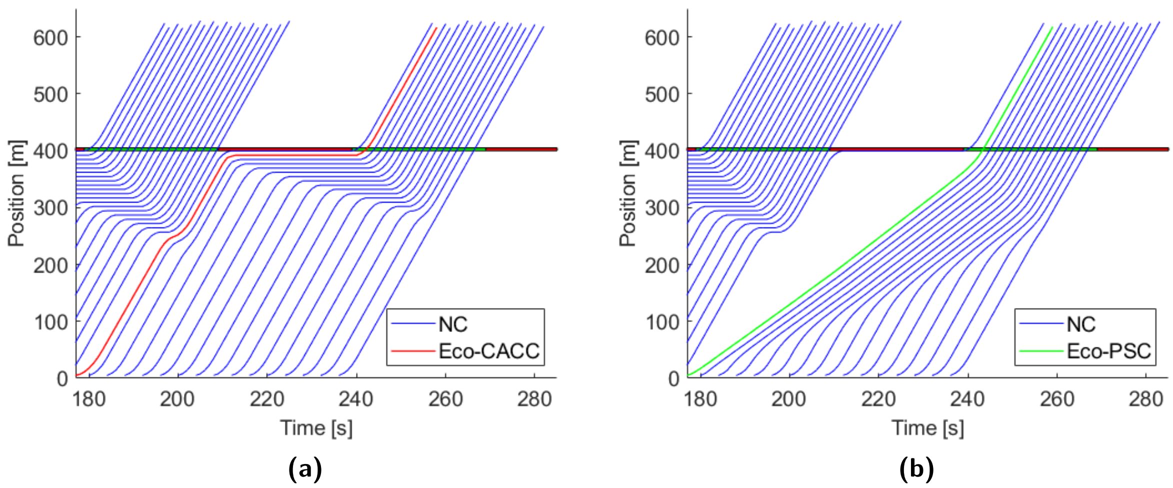

Figure 4-7: Vehicle trajectories around the signalized intersection in Case study II: (a) the blue lines represent the non-controlled vehicles and the red line represents the CACC vehicle, (b) the blue lines represent the non-controlled vehicles and the green line represents the PSC vehicle.

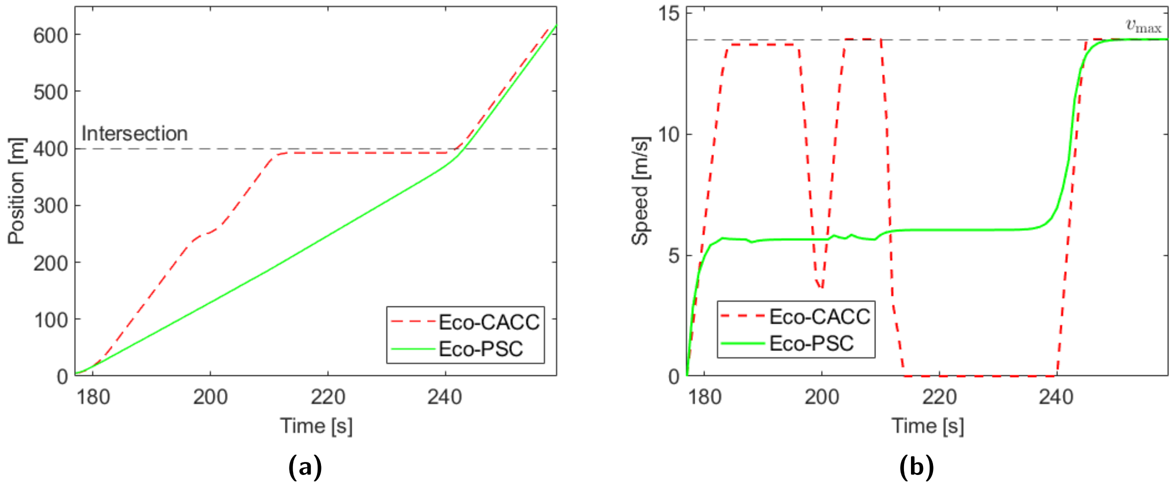

Figure 4-8: Eco-driving in Case study II: (a) comparison of vehicle trajectories of the controlled vehicle, (b) comparison of speed profiles of the controlled vehicle.

Table 4-4: Performance evaluation of the Eco-PSC algorithm in terms of fuel consumption, travel time, maximum computation time and relative change in fuel consumption and travel time compared to the benchmark algorithm in Case study II. Furthermore, the average fuel consumption and travel time of the non-controlled vehicles related to the eco-driving strategies, denoted by $\mathrm{NC_{CACC}}$ and $\mathrm{NC_{PSC}}$, are also presented.

Control	FC [ml]	TT [s]	$\mathrm{FC_{rel}}$ [%]	$\mathrm{TT_{rel}}$ [%]	$\mathrm{CT_{max}}$ [s]
Eco-CACC	112.07	80.88	-	-	-
Eco-PSC	79.40	81.81	-29.15	+1.15	0.53
$\mathrm{NC_{CACC}}$	86.95	64.97	-	-	-
$\mathrm{NC_{PSC}}$	84.67	65.34	-2.62	+0.57	-

driving with the Eco-CACC algorithm is shorter. Compared to the benchmark algorithm, the travel time of the PSC vehicle is increased by 1.15%. An explanation for the increase in travel time can be found in Section 4-1-2.

Figure 4-8b compares the speed profiles of the controlled vehicle for the two eco-driving algorithms. The speed profile computed by the Eco-PSC algorithm is much smoother than the benchmark algorithm. For the benchmark algorithm, the cruise speed considering the first queue is 13.68 m/s. Then, since the benchmark algorithm underestimates the queue the speed drops for approximately 8 seconds. An explanation for this inaccurate estimation is that the queue length is predicted based on the FD, which was calibrated for the PSC method. Subsequently, the vehicle stops for 35 seconds as the algorithm does not account for residual queues. When being controlled by the Eco-PSC algorithm, the vehicle cruises at a speed of approximately 5.84 m/s and does not stop upstream of the intersection. Nonetheless, the speed of the vehicle slightly fluctuates as the dynamically changing queue length introduces some speed changes.

As presented in Table 4-4, the fuel consumption of the controlled vehicle is 112.07 ml for the benchmark algorithm and 79.40 ml for the Eco-PSC algorithm. Hence, the Eco-PSC algorithm is the more efficient control method, with reductions in fuel consumption levels as high as 29.15%. The Eco-PSC algorithm also smooths the trajectories of the non-controlled vehicles besides the controlled vehicle (as shown in Figure 4-7). As a result, the Eco-PSC algorithm reduces the average fuel consumption levels by 2.62%. Finally, a maximum computation time of 0.53 seconds per sampling interval was observed.

4-5 Case study III - upstream spillback

In this section, the effectiveness of the Eco-PSC algorithm in oversaturated traffic conditions where the controlled vehicle causes upstream spillback is evaluated. The demand profile of Figure 4-3c is loaded to the intersection for 300 seconds and the probe vehicle enters the network at $t = 160$ seconds.

Figure 4-9 illustrates the trajectories of all vehicles before and after applying the Eco-PSC algorithm over two signal cycles, where the traffic light is located at 400 meters. In Figure 4-9a, without control, the probe vehicle merely follows its leader and comes twice to a complete stop upstream of the intersection waiting for the traffic signal to release the queues. While in Figure 4-9b, the Eco-PSC algorithm ensures that the vehicle can cruise towards the intersection and catch the tail of the second queue when it is discharged. This way, the controlled vehicle can avoid incurring a complete stop ahead of the traffic signal and follow the calculated trajectory. However, the vehicle causes depart delays on its following vehicles with an average value of 6.93 seconds.

Figure 4-10 compares the true vehicle inflow with and without control to the desired vehicle inflow, i.e. the demand. The figure demonstrates the algorithm changes the upstream cumulative flow curves after the controlled vehicle has entered the link. Hence, the controlled

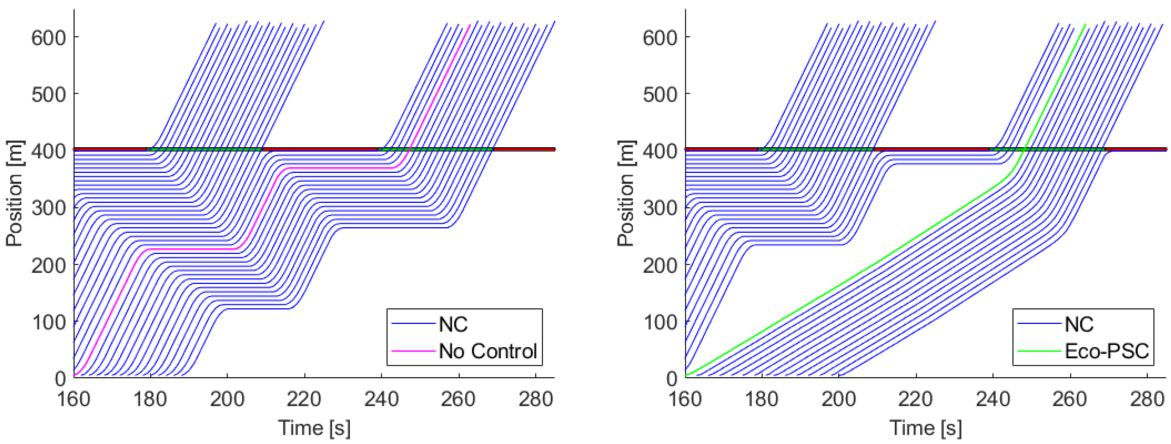

(a) (b)

Figure 4-9: Vehicle trajectories around the signalized intersection in Case study III: (a) the blue lines represent the non-controlled vehicles and the purple line represents the probe vehicle, (b) the blue lines represent the non-controlled vehicles and the green line represents the PSC vehicle.

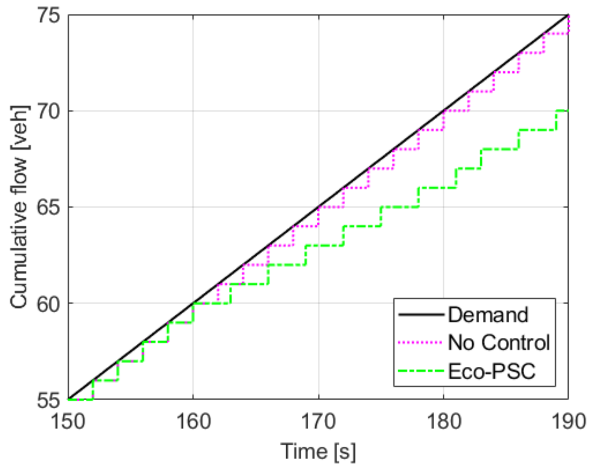

Figure 4-10: The true vehicle inflow with and without control compared to the desired vehicle inflow in Case study III.

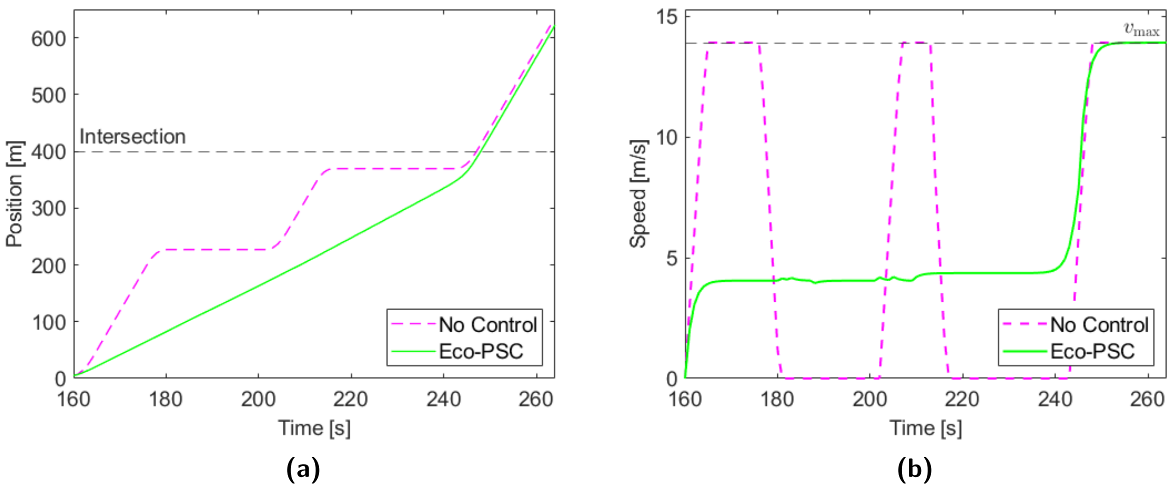

Figure 4-11: Eco-driving in Case study III: (a) comparison of vehicle trajectories of the probe vehicle, (b) comparison of speed profiles of the probe vehicle.

vehicle causes upstream spillback that does not occur without control. To prevent upstream spillback, one should involve upstream demand-related constraints into the control framework.

Figure 4-11a compares the trajectories of the probe vehicle before and after applying the Eco-PSC algorithm. Compared to the trajectory without control, the trajectory is much smoother when the algorithm is implemented. Nevertheless, the travel time of the vehicle driving with the algorithm is increased by 0.93%. An explanation for the increase in driving time can be found in Section 4-1-2. Figure 4-11b compares the speed profiles of the probe vehicle before and after applying the Eco-PSC algorithm. Without control, the vehicle stops upstream of the traffic signal for 21 and 26 seconds, respectively. While the controlled vehicle accelerates to a cruise speed of approximately 4.21 m/s and crosses the intersection without stopping. Nevertheless, the dynamically changing queue length introduces some speed changes.

Table 4-5: Performance evaluation of the Eco-PSC algorithm in terms of fuel consumption, travel time, maximum computation time and relative change in fuel consumption and travel time compared to the No Control policy in Case study III. Furthermore, the average fuel consumption and travel time of the last non-controlled vehicle is also presented.

Control	FC [ml]	TT [s]	FC_{rel} [%]	TT_{rel} [%]	CT_{max} [s]
No Control	124.60	102.50	-	-	-
Eco-PSC	92.50	103.45	-25.76	+0.93	0.64
Last vehicle_{NC}	121.05	96.05	-	-	-
Last vehicle_{PSC}	124.61	128.34	+2.94	+33.62	-

As presented in Table 4-5, the fuel consumption levels before and after implementing the algorithm are 124.60 ml and 92.50 ml, respectively. This indicates the algorithm reduces fuel consumption levels by 25.76%. Furthermore, a maximum computation time of 0.64 seconds per sampling interval was observed. However, the controlled vehicle causes negative impacts on its following vehicles as the last vehicle is unable to cross the intersection during the same green window as planned (as seen in Figure 4-9). Because of the overestimation of queues, the last vehicle in the figure runs into a red signal and experiences an increase in fuel consumption and travel time by 2.94% and 33.62%, respectively. In terms of system performance, the suggested speed profile increases the queue length of the next cycle. As a result, the controlled vehicle deteriorates the overall system performance. To avoid negative impacts on following vehicles, one could suggest the controlled vehicle to cross the intersection before a certain time.

4-6 Case study IV - market penetration rates

In this section, the impact of market penetration rates (MPRs) on the Eco-PSC algorithm performance is investigated. A constant demand flow of $q_d = 900$ veh/h is loaded to the intersection for 300 seconds and the MPR varies from 0 to 100%. The controlled vehicles for different MPRs are randomly chosen with the *randperm* command in MATLAB.

Figure 4-12 shows the average network-wide fuel consumption levels considering different MPRs. As can be seen in the figure, the benefits grow with increasing MPRs of controlled vehicles until it levels off at about 80% MPR. At 80% MPR, the average fuel consumption is reduced by 15.72%. In the simulations, the algorithm smooths the trajectories of the controlled vehicles, while simultaneously smoothing the movements of some non-controlled vehicles due to car-following behavior, further reducing the overall fuel consumption levels. Even at an MPR of 20%, significant benefits are observed. This indicates the proposed algorithm can be implemented even with low MPRs of controlled vehicles.

Figure 4-13 shows the average network-wide travel times considering different MPRs. With higher MPRs, the travel time is longer as demonstrated in the figure. At 100% MPR, the travel time is increased by 1.49%. Nonetheless, this is expected as explained in Section 4-1-2.

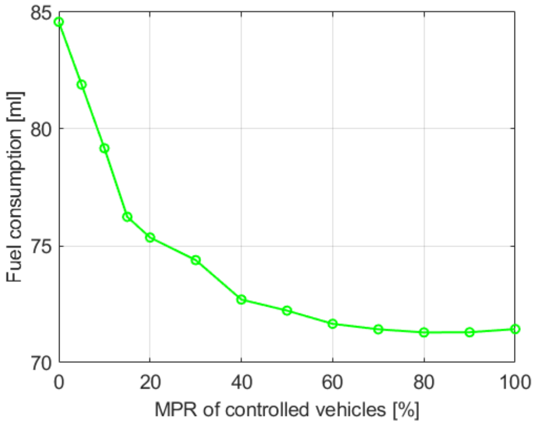

Figure 4-12: Fuel consumption for different market penetration rates in Case study IV.

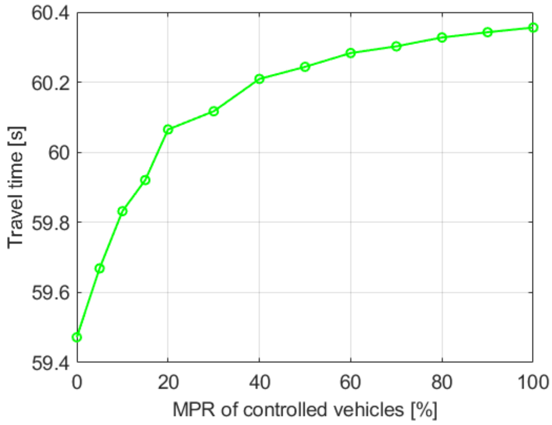

Figure 4-13: Travel time for different market penetration rates in Case study IV.

4-7 Case study V - stochastic traffic behavior

In this section, the impact of stochasticity in traffic behavior on the Eco-PSC algorithm performance is investigated. The stochasticity is added in the form of driver imperfection, i.e. the non-controlled vehicles deviate from the legal speed limit and do not apply constant throttle. In this case study, a speed distribution where 95% of the vehicles drive between 80% and 120% of the legal speed limit is chosen [61].

4-7-1 Single queue

In the first step, the traffic scenario from Case study I is reconsidered. Hence, the demand profile of Figure 4-3a is loaded to the intersection for 300 seconds and the controlled vehicle enters the network at $t = 144$ seconds.

Figure 4-14 illustrates the trajectories of all vehicles for the two eco-driving algorithms over one cycle length, where the traffic signal is located at 400 meters. A significant difference compared to Case study I is that the queue length is increased by one vehicle. Figure 4-14a shows the vehicle trajectories after implementing the Eco-CACC algorithm. Similar to the first case study, the controlled vehicle slows down to approach the intersection and runs into the vehicle waiting queue. While in Figure 4-14b, the Eco-PSC algorithm ensures that the vehicle can cruise towards the traffic signal and just catch the tail of the queue when it is released.

Figure 4-15a compares the trajectories of the controlled vehicle for the two eco-driving algorithms. As depicted in the figure, the travel time of both vehicles is practically identical. However, the trajectory is smoother when the Eco-PSC algorithm is implemented as the benchmark algorithm is unable to accurately estimate the tail location of the queue. Figure 4-15b compares the speed profiles of the controlled vehicle for the two eco-driving algorithms. Compared to Case study I, only the cruise speed of the PSC vehicle is lower, i.e. 7.78 m/s. Because of the receding horizon approach, the Eco-PSC algorithm can deal with uncertainties and calculate the cruise speed with new information about the measurements. Moreover, the

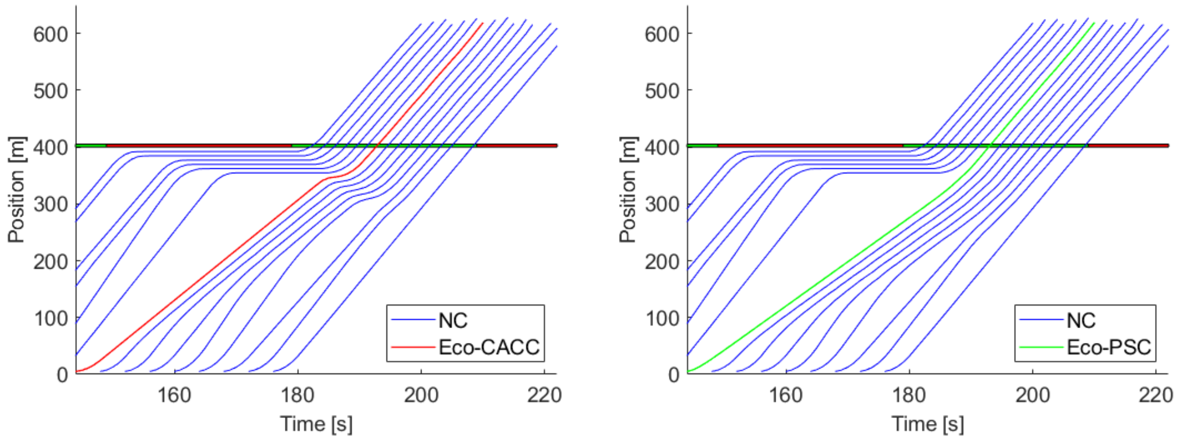

(a) **(b)**

Figure 4-14: Vehicle trajectories around the signalized intersection for the single queue scenario in Case study V: (a) the blue lines represent the non-controlled vehicles and the red line represents the CACC vehicle, (b) the blue lines represent the non-controlled vehicles and the green line represents the PSC vehicle.

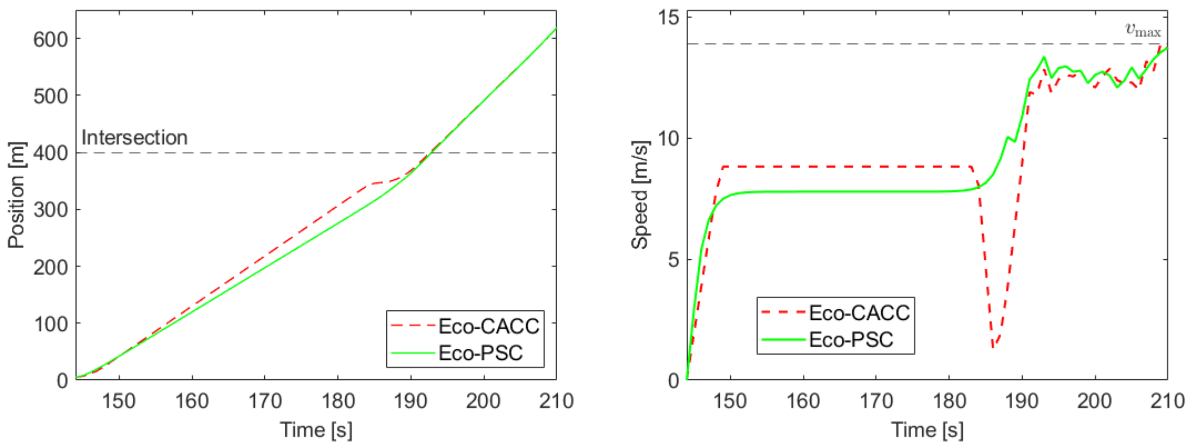

(a) **(b)**

Figure 4-15: Eco-driving for the single queue scenario in Case study V: (a) comparison of vehicle trajectories of the controlled vehicle, (b) comparison of speed profiles of the controlled vehicle.

speed of the CACC vehicle drops sharply for approximately 7 seconds due to the inaccurate estimation of the queue. For the Eco-PSC algorithm the speed slightly changes, although this is minimal because of the overestimation of the queue. Nevertheless, after 190 seconds the driver imperfection of the preceding vehicle introduces frequent speed changes for both algorithms.

As presented in Table 4-6, the fuel consumption of the controlled vehicle is 82.09 ml for the benchmark algorithm and 75.90 ml for the Eco-PSC algorithm. Hence, the Eco-PSC algorithm is the more efficient control method, reducing the fuel consumption levels by 7.54%. In addition, the Eco-PSC algorithm smooths the trajectories of the non-controlled vehicles

Table 4-6: Performance evaluation of the Eco-PSC algorithm in terms of fuel consumption, travel time, maximum computation time and relative change in fuel consumption and travel time compared to the benchmark algorithm for the single queue scenario in Case study V. Furthermore, the average fuel consumption and travel time of the non-controlled vehicles related to the eco-driving strategies, denoted by $\mathrm{NC_{CACC}}$ and $\mathrm{NC_{PSC}}$, are also presented.

Control	FC [ml]	TT [s]	$\mathrm{FC_{rel}}$ [%]	$\mathrm{TT_{rel}}$ [%]	$\mathrm{CT_{max}}$ [s]
Eco-CACC	82.09	65.71	-	-	-
Eco-PSC	75.90	65.69	-7.54	-0.03	0.45
$\mathrm{NC_{CACC}}$	93.96	64.80	-	-	-
$\mathrm{NC_{PSC}}$	91.46	64.77	-2.66	-0.05	-

(as seen in Figure 4-14). The example above demonstrates that the algorithm reduces the average fuel consumption by 2.66%. Lastly, a maximum computation time of 0.45 seconds per sampling interval was observed.

4-7-2 Running into a red light

Secondly, consider the scenario where the controlled vehicle is the last vehicle that can traverse the intersection during the current green phase in perfect driving conditions. Then due to driver imperfection of the preceding vehicle, the controlled vehicle suddenly runs into a red signal and has to wait for the next green window to proceed through the intersection. In this scenario, a constant demand flow of $q_d = 900$ veh/h is loaded to the intersection for 300 seconds and the controlled vehicle enters the network at $t = 116$ seconds.

Figure 4-16 illustrates the trajectories of all vehicles for the two eco-driving algorithms over one signal cycle, where the traffic light is located at 400 meters. Figure 4-16a shows the vehicle trajectories after implementing the Eco-CACC algorithm. As can be seen in the figure, the controlled vehicle cruises towards the intersection and runs into the red traffic light. Consequently, the vehicle has to come to a complete stop and idle in front of the signal before it can continue its path. While in Figure 4-16b, the Eco-PSC algorithm adjusts its trajectory once the MPC controller predicts the vehicle can no longer cross the intersection during the current green phase. This way, the vehicle can prevent idling upstream of the traffic signal.

Figure 4-17a compares the trajectories of the controlled vehicle for the two eco-driving algorithms. The trajectory is slightly smoother when the Eco-PSC algorithm is implemented. Nevertheless, the travel time of the vehicle driving with the Eco-CACC algorithm is shorter. Compared to the benchmark algorithm, the travel time of the PSC vehicle is increased by 1.65%. Figure 4-17b compares the speed profiles of the controlled vehicle for the two eco-driving algorithms. As can be seen in the figure, both algorithms accelerate to cruise speed. After 141 seconds the speed of the CACC vehicle fluctuates due to driver imperfection of the preceding vehicle. Subsequently, the CACC vehicle runs into the red traffic light and comes to a complete stop for 28 seconds. The Eco-PSC algorithm exhibits indecisive behavior as it is uncertain if the vehicle can cross the intersection during the current green phase. Then,

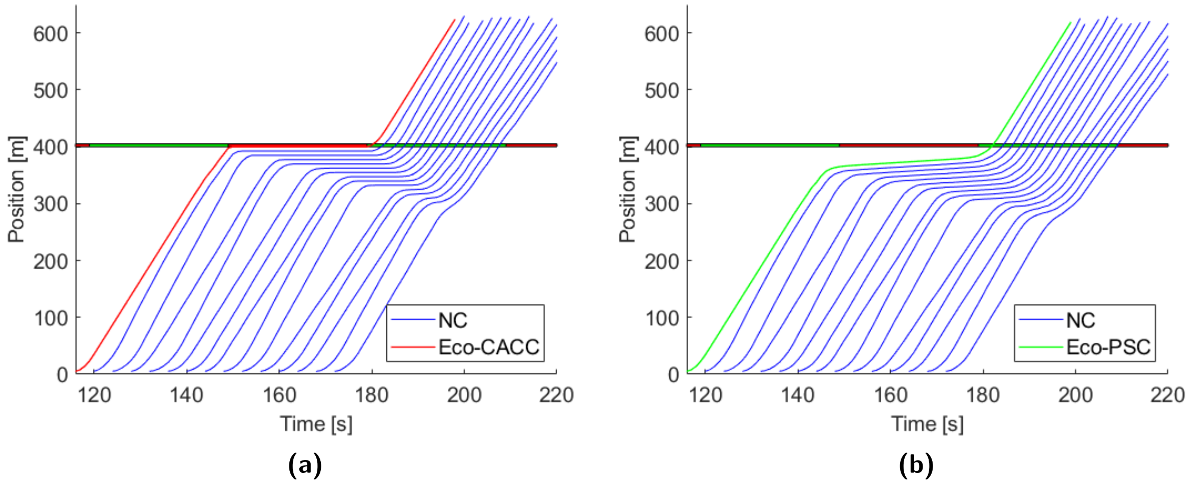

Figure 4-16: Vehicle trajectories around the signalized intersection for the red light scenario in Case study V: (a) the blue lines represent the non-controlled vehicles and the red line represents the CACC vehicle, (b) the blue lines represent the non-controlled vehicles and the green line represents the PSC vehicle.

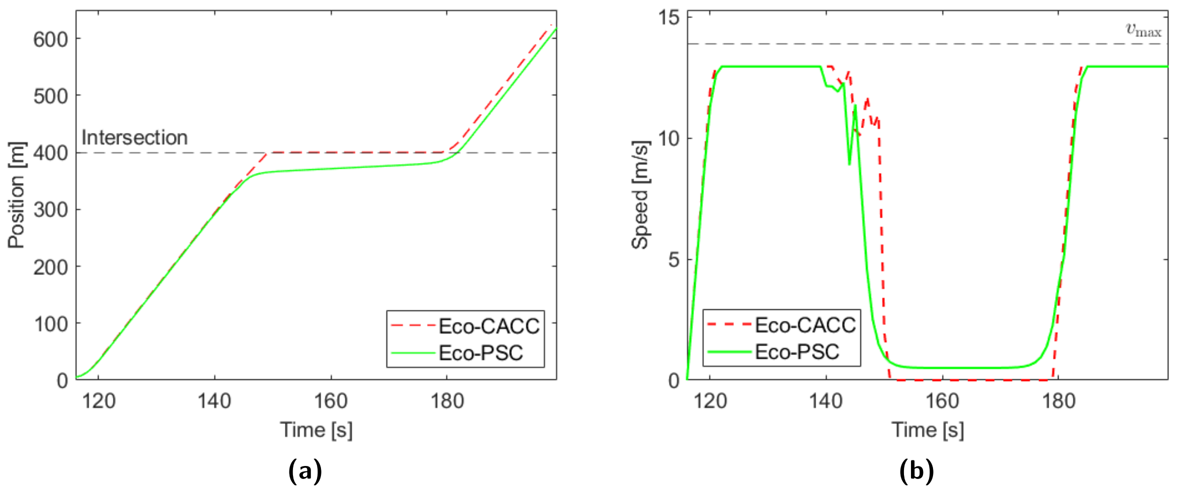

Figure 4-17: Eco-driving for the red light scenario in Case study V: (a) comparison of vehicle trajectories of the controlled vehicle, (b) comparison of speed profiles of the controlled vehicle.

at $t = 145$ seconds the algorithm estimates the vehicle can no longer cross the intersection during the current green window and adjusts the cruise speed to 0.50 m/s. However, this speed is below the speed of a pedestrian (i.e. 1.24 m/s [66]) and therefore the vehicle can be considered stopped. To prevent indecisive behavior, one could set a speed threshold value to define when the traffic state switches from free-flow to congested. This way, the algorithm can adjust the cruise speed accordingly.

As presented in Table 4-7, the fuel consumption of the controlled vehicle is 97.24 ml for the benchmark algorithm and 96.29 ml for the Eco-PSC algorithm. This means that in this example, the benefits of the Eco-PSC algorithm for the controlled vehicle are negligible.

Table 4-7: Performance evaluation of the Eco-PSC algorithm in terms of fuel consumption, travel time, maximum computation time and relative change in fuel consumption and travel time compared to the benchmark algorithm for the red light scenario in Case study V. Furthermore, the average fuel consumption and travel time of the non-controlled vehicles related to the eco-driving strategies, denoted by $\mathrm{NC_{CACC}}$ and $\mathrm{NC_{PSC}}$, are also presented.

Control	FC [ml]	TT [s]	$\mathrm{FC_{rel}}$ [%]	$\mathrm{TT_{rel}}$ [%]	$\mathrm{CT_{max}}$ [s]
Eco-CACC	97.24	81.35	-	-	-
Eco-PSC	96.29	82.69	-0.98	+1.65	0.47
$\mathrm{NC_{CACC}}$	114.75	66.36	-	-	-
$\mathrm{NC_{PSC}}$	112.32	67.52	-2.12	+1.75	-

Nevertheless, the PSC vehicle exerts a positive influence on its following vehicles, since the average fuel consumption levels are decreased by 2.12%. Finally, a maximum computation time of 0.47 seconds per sampling interval was observed.

Chapter 5

Conclusions and future work

This thesis designed a predictive speed control (PSC) strategy to reduce the fuel consumption of vehicles proceeding through signalized intersections. The algorithm utilizes signal phase and timing (SPaT) information obtained through infrastructure-to-vehicle (I2V) communication and real-time passing data collected using induction loop detectors to compute optimal speed profiles. The algorithm estimates traffic imposed constraints based on traffic signal information, cumulative flow curves and the LWR-model. Microscopic traffic simulations have been run in SUMO with realistic traffic inputs, such as signal timing and demand profiles. Various case studies have been conducted to evaluate the effectiveness of the developed Eco-PSC algorithm. This chapter presents the key conclusions of the simulation results in Section 5-1 and includes further discussion on future work in Section 5-2.

5-1 Conclusions

The main goal of this thesis was defined as follows:

> To develop a real-time implementable PSC strategy for vehicles proceeding through signalized intersections to reduce fuel consumption while considering queue constraints.

To accomplish the main research objective, two subquestions were formulated. These questions will be answered first:

1. *What is an accurate method to estimate queue propagation in the vicinity of signalized intersections?*

   Many traffic flow models can be applied to estimate the queuing effect and derive the spatial and temporal constraints. The LWR is a kinematic wave model that describes traffic dynamics on roads. The theory of kinematic waves combines the conservation of vehicles principle together with a fundamental diagram of traffic flow. Newell uses kinematic wave theory to directly evaluate the cumulative flow for points in space-time.

The benefit of this method is that the cumulative flow for the full space-time domain can be estimated from initial and boundary conditions without evaluation at intermediate locations and times. Based on Newell's simplified method, an efficient and accurate procedure to estimate the future cumulative flow curves and identify the restrictive red periods is developed. Thereafter, the spatial and temporal restrictions for the controlled vehicle can be determined based on the future cumulative flow curves, the LWR-model and the cumulative flow value of the controlled vehicle.

2. *How can the queue constraints be integrated into the control framework such that it operates in various traffic conditions?*

   The estimation accuracy and efficiency of traffic and signal conditions are critical for the effectiveness of the optimal speed profile provided by the PSC strategy. Residual queues caused by oversaturated demand flows generate traffic fluctuations and complete stops for the controlled vehicle. To counteract this problem, the proposed algorithm introduces a point in the space-time domain for each restrictive red period. This point represents the spatial and temporal constraint imposed by the presence of the queue on the signalized road. To avoid idling in the queue, the controlled vehicle should not pass the location of this point before the dissipation time of the queue.

In the first case study, the proposed algorithm was compared to the benchmark algorithm in undersaturated conditions where queues can completely dissolve in a single cycle. This case study showed the proposed algorithm can more accurately estimate the tail location of the queue. This results in a reduction in fuel consumption by 4.35%, although the travel time is increased by 1.14%. In the second case study, the proposed algorithm was compared to the benchmark algorithm in oversaturated conditions where residual queues are formed. Due to the impact of residual queues, the benchmark algorithm does not operate efficiently. In contrast, the Eco-PSC algorithm identifies the restrictive red periods and introduces a constraint for each queue. This way, the Eco-PSC algorithm can achieve a reduction in fuel consumption as high as 29.15%. However, this fuel consumption saving is at the expense of an increase in driving time by 1.15%. In the third case study, the proposed algorithm causes upstream spillback that does not occur without control. The controlled vehicle causes depart delays on its following vehicles with an average value of 6.93 seconds. Moreover, the suggested speed trajectory causes negative impacts on following vehicles in terms of additional fuel consumption and travel time.

In the fourth case study, the impact of market penetration rates (MPRs) on the proposed algorithm performance was investigated. This case study showed that the benefits grew with increasing MPRs of controlled vehicles until it leveled off at about 80% MPR. At an MPR of 80%, fuel consumption savings of 15.72% were achieved. However, higher MPRs also lead to an increase in travel time by 1.49% at 100% MPR. In the last case study, the impact of stochastic traffic behavior on the proposed algorithm performance was investigated. Because of the receding horizon approach, the Eco-PSC algorithm is relatively robust to uncertainties and can calculate the cruise speed with new information about the measurements. In the first part of this case study, the proposed algorithm was able to accurately calculate the tail location of the queue and achieve a fuel consumption saving of 7.54%, while causing no adverse effect on the travel time. In the second part of this case study, the benefits of the proposed algorithm compared to the benchmark algorithm were negligible for the controlled vehicle.

In conclusion, the proposed algorithm can accurately estimate queue propagation and operate in various traffic conditions. In addition, the proposed algorithm smooths the trajectories of the non-controlled vehicles due to car-following behavior, which further reduces the fuel consumption levels in the network. Furthermore, the maximum computation time found in the various case studies was less than the sampling interval of the system, which makes the MPC controller real-time implementable. However, the control framework should be further improved in order to realize the Eco-PSC algorithm.

5-2 Recommendations for future work

Based on the simulation results, several directions for future research can be recommended to improve the Eco-PSC algorithm.

Improvements to the framework The primary recommendation would be to further improve the control framework. Here, some suggestions are summarized:

- Set a speed threshold value to prevent indecisive behavior.
- Utilize a multi-start algorithm to increase the chance of finding a global solution.
- Integrate a constraint to avoid negative impacts on following vehicles.
- Include upstream demand-related constraints to prevent additional upstream spillback.

Note that in the latter, the term additional is used as the MPC controller should prevent upstream spillback that is caused by the controlled vehicle but would not have occurred otherwise. The developed method is particularly suitable for including upstream restrictions in contrast to other methods like the benchmark algorithm. The upstream queue length and discharge time can be calculated in a similar manner as the downstream supply-related constraints but viewed from the perspective of the upstream link boundary. For this, one should draw a w-wave every time a new vehicle enters the link after the controlled vehicle and determine if additional upstream spillback would occur, see Figure 5-1. In case of additional upstream spillback, the controlled vehicle is suggested to drive at a relatively faster departure speed to allow more upstream vehicles to enter the link.

Traffic signal and future inflow information Traffic signal information was in this thesis included via a fixed and known signal timing. Extensions could be to implement traffic-actuated signals and take the stochastic nature of traffic signal timing into account, where the probability of a green light is predicted based on the current phase and the average signal timing data [67]. Moreover, the phase transition can be extended by including the amber phase in addition to the red and green phases, which would make the simulations closer to reality. Furthermore, in the simulation case studies, perfect knowledge of the future demand was assumed, i.e. we know when other upstream vehicles enter the link. Nevertheless, one can also introduce an uncertainty in the demand, where the demand can be described by a probability density function.

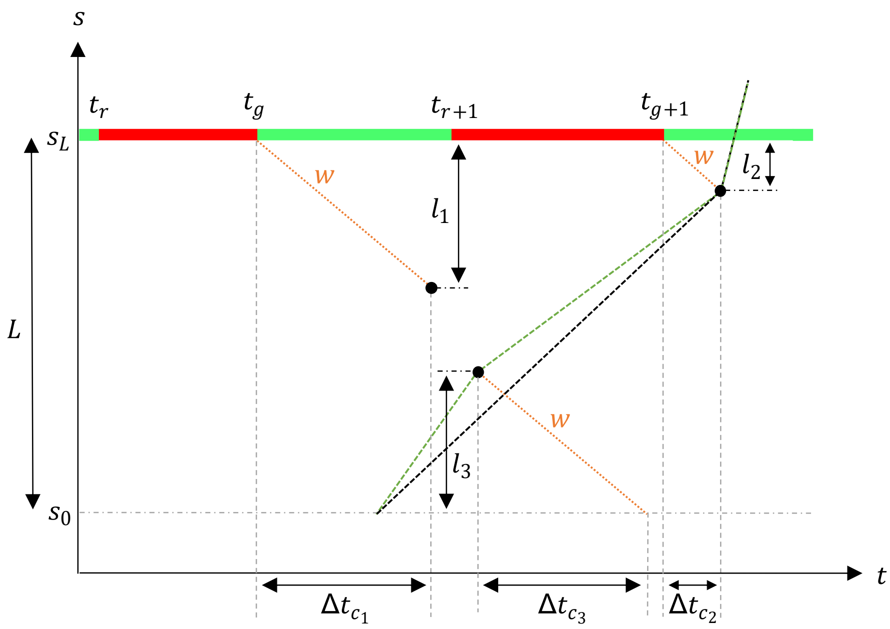

Figure 5-1: Trajectories of shockwaves and the controlled vehicle for the formulation of the upstream demand-related constraints. The dashed black line represents the trajectory without consideration of additional upstream spillback and the dashed green line represents the trajectory with consideration of additional upstream spillback.

Performance on larger and more realistic traffic networks The algorithm minimizes fuel consumption levels of vehicles traversing a single intersection, limiting its application on arterial roads with multiple consecutive signalized intersections. Hence, larger networks with two, four or eight intersections should be implemented to expand the feasibility of the algorithm. Moreover, only single-lane roads were considered to prevent dealing with complex lane-changing behavior. However, a more realistic intersection layout comprises links where the roads upstream and downstream of the intersection consist of more than one lane. Thus, it would be intriguing to see how the system performance and computational complexity change by considering multi-lane roads and multiple consecutive intersections in the optimization logic.

Human and wireless communication factors The effectiveness of eco-driving strategies is deeply related to the behavioral adjustment of the driver to the cruise control system. If drivers refuse to comply with the provided speed advice, the advantage of the application diminishes. Hence, the driver's compliance with the system, which depends on situational factors, acceptance, personal traits and trust [50], remains a critical factor for realizing the benefits of eco-driving algorithms. Furthermore, the effects of wireless communication, e.g. communication delay, transmission range and packet loss, on the algorithm performance should be further analyzed.

Bibliography

[1] L. Byrne, V. Bach, and M. Finkbeiner, "Urban transport assessment of emissions and resource demand of climate protection scenarios," *Cleaner Environmental Systems*, vol. 2, p. 100019, 2021.

[2] B. R. Singh and O. Singh, "Global trends of fossil fuel reserves and climate change in the 21st century," *Fossil Fuel and the Environment*, vol. 8, 2012.

[3] S. L. Jamson, D. L. Hibberd, and A. H. Jamson, "Drivers' ability to learn eco-driving skills; effects on fuel efficient and safe driving behaviour," *Transportation Research Part C: Emerging Technologies*, vol. 58, pp. 657–668, 2015. Technologies to support green driving.

[4] S. M. Pampel, S. L. Jamson, D. L. Hibberd, and Y. Barnard, "How I reduce fuel consumption: An experimental study on mental models of eco-driving," *Transportation Research Part C: Emerging Technologies*, vol. 58, pp. 669–680, 2015.

[5] B. Khondaker and L. Kattan, "Variable speed limit: A microscopic analysis in a connected vehicle environment," *Transportation Research Part C: Emerging Technologies*, vol. 58, pp. 146–159, 2015.

[6] E. Larsson, G. Sennton, and J. Larson, "The vehicle platooning problem: Computational complexity and heuristics," *Transportation Research Part C: Emerging Technologies*, vol. 60, pp. 258–277, 2015.

[7] J. Sun and H. X. Liu, "Stochastic eco-routing in a signalized traffic network," *Transportation Research Part C: Emerging Technologies*, vol. 59, pp. 32–47, 2015. Special Issue on International Symposium on Transportation and Traffic Theory.

[8] M. Barth and K. Boriboonsomsin, "Energy and emissions impacts of a freeway-based dynamic eco-driving system," *Transportation Research Part D: Transport and Environment*, vol. 14, no. 6, pp. 400–410, 2009. The interaction of environmental and traffic safety policies.

[9] D. Schrank, B. Eisele, and T. Lomax, “2019 urban mobility report,” tech. rep., Texas Transportation Institute, 2019.

[10] U.S. Department of Transportation, “The intelligent transportation systems for traffic signal control deployment benefits and lessons learned,” tech. rep., Washington, DC, 2007.

[11] National Transportation Operations Coalition, “National traffic signal report card,” tech. rep., Washington, DC, 2007.

[12] B. Asadi and A. Vahidi, “Predictive cruise control: Utilizing upcoming traffic signal information for improving fuel economy and reducing trip time,” *IEEE Transactions on Control Systems Technology*, vol. 19, no. 3, pp. 707–714, 2011.

[13] D. Sun and L. Elefteriadou, “Lane-changing behavior on urban streets: A focus group-based study,” *Applied Ergonomics*, vol. 42, no. 5, pp. 682–691, 2011.

[14] C. Sun, J. Guanetti, F. Borrelli, and S. J. Moura, “Optimal eco-driving control of connected and autonomous vehicles through signalized intersections,” *IEEE Internet of Things Journal*, vol. 7, no. 5, pp. 3759–3773, 2020.

[15] H. Dong, W. Zhuang, G. Yin, H. Chen, and Y. Wang, “Energy-optimal velocity planning for connected electric vehicles at signalized intersection with queue prediction,” in *2020 IEEE/ASME International Conference on Advanced Intelligent Mechatronics (AIM)*, pp. 238–243, 2020.

[16] H. Chen, L. Guo, H. Ding, Y. Li, and B. Gao, “Real-time predictive cruise control for eco-driving taking into account traffic constraints,” *IEEE Transactions on Intelligent Transportation Systems*, vol. 20, no. 8, pp. 2858–2868, 2019.

[17] B. HomChaudhuri, A. Vahidi, and P. Pisu, “Fast model predictive control-based fuel efficient control strategy for a group of connected vehicles in urban road conditions,” *IEEE Transactions on Control Systems Technology*, vol. 25, no. 2, pp. 760–767, 2017.

[18] X. He, H. X. Liu, and X. Liu, “Optimal vehicle speed trajectory on a signalized arterial with consideration of queue,” *Transportation Research Part C: Emerging Technologies*, vol. 61, pp. 106 – 120, 2015.

[19] H. Yang, F. Almutairi, and H. Rakha, “Eco-driving at signalized intersections: A multiple signal optimization approach,” *IEEE Transactions on Intelligent Transportation Systems*, vol. 22, no. 5, pp. 2943–2955, 2021.

[20] M. A. S. Kamal, M. Mukai, J. Murata, and T. Kawabe, “Model predictive control of vehicles on urban roads for improved fuel economy,” *IEEE Transactions on Control Systems Technology*, vol. 21, no. 3, pp. 831–841, 2013.

[21] S. G. Dehkordi, G. S. Larue, M. E. Cholette, A. Rakotonirainy, and H. A. Rakha, “Ecological and safe driving: A model predictive control approach considering spatial and temporal constraints,” *Transportation Research Part D: Transport and Environment*, vol. 67, pp. 208–222, 2019.

[22] J. B. Rawlings, D. Q. Mayne, and M. Diehl, *Model predictive control: theory, computation, and design.* Nob Hill Publishing, 2 ed., 2017.

[23] S. Qin and T. A. Badgwell, "A survey of industrial model predictive control technology," *Control Engineering Practice*, vol. 11, no. 7, pp. 733–764, 2003.

[24] Z. Wang, G. Wu, P. Hao, and M. J. Barth, "Cluster-wise cooperative eco-approach and departure application for connected and automated vehicles along signalized arterials," *IEEE Transactions on Intelligent Vehicles*, vol. 3, no. 4, pp. 404–413, 2018.

[25] Z. Wang, G. Wu, and M. J. Barth, "Cooperative eco-driving at signalized intersections in a partially connected and automated vehicle environment," *IEEE Transactions on Intelligent Transportation Systems*, vol. 21, no. 5, pp. 2029–2038, 2020.

[26] X. Wu, X. He, G. Yu, A. Harmandayan, and Y. Wang, "Energy-optimal speed control for electric vehicles on signalized arterials," *IEEE Transactions on Intelligent Transportation Systems*, vol. 16, no. 5, pp. 2786–2796, 2015.

[27] H. Yang, H. Rakha, and M. V. Ala, "Eco-cooperative adaptive cruise control at signalized intersections considering queue effects," *IEEE Transactions on Intelligent Transportation Systems*, vol. 18, no. 6, pp. 1575–1585, 2017.

[28] V. L. Knoop, *Traffic Flow Theory: An introduction with exercises.* TU Delft Open, 3 ed., 2021.

[29] Y. Makigami, G. F. Newell, and R. Rothery, "Three-dimensional representation of traffic flow," *Transportation Science*, vol. 5, no. 3, pp. 302–313, 1971.

[30] C. F. Daganzo, *Fundamentals of transportation and traffic operations.* Emerald Publishing, 1 ed., 1997.

[31] M. J. Lighthill and G. B. Whitham, "On kinematic waves ii. a theory of traffic flow on long crowded roads," *Proceedings of the Royal Society of London. Series A. Mathematical and Physical Sciences*, vol. 229, no. 1178, pp. 317–345, 1955.

[32] P. I. Richards, "Shock waves on the highway," *Operations Research*, vol. 4, no. 1, pp. 42–51, 1956.

[33] T. Seo, A. M. Bayen, T. Kusakabe, and Y. Asakura, "Traffic state estimation on highway: A comprehensive survey," *Annual Reviews in Control*, vol. 43, pp. 128–151, 2017.

[34] I. Yperman, *The Link Transmission Model for dynamic network loading.* PhD thesis, Katholieke Universiteit Leuven, 2007.

[35] G. Newell, "A simplified theory of kinematic waves in highway traffic, part I: General theory," *Transportation Research Part B: Methodological*, vol. 27, no. 4, pp. 281 – 287, 1993.

[36] G. F. Newell, "A simplified theory of kinematic waves in highway traffic, part II: Queueing at freeway bottlenecks," *Transportation Research Part B: Methodological*, vol. 27, no. 4, pp. 289–303, 1993.

[37] G. Newell, "A simplified theory of kinematic waves in highway traffic, part III: Multi-destination flows," *Transportation Research Part B: Methodological*, vol. 27, no. 4, pp. 305–313, 1993.

[38] P.B.C. van Erp, *Relative Flow Data: New Opportunities for Traffic State Estimation*. PhD thesis, Delft University of Technology, 2020.

[39] G. Comert, "Queue length estimation from probe vehicles at isolated intersections: Estimators for primary parameters," *European Journal of Operational Research*, vol. 252, no. 2, pp. 502 – 521, 2016.

[40] Z. Wang, L. Zhu, B. Ran, and H. Jiang, "Queue profile estimation at a signalized intersection by exploiting the spatiotemporal propagation of shockwaves," *Transportation Research Part B: Methodological*, vol. 141, pp. 59 – 71, 2020.

[41] P. Dell'Olmo and P. B. Mirchandani, "A model for real-time traffic coordination using simulation based optimization," in *Advanced Methods in Transportation Analysis* (L. Bianco and P. Toth, eds.), pp. 525–546, Springer Berlin Heidelberg, 1996.

[42] R. Trayford, B. Doughty, and M. Wooldridge, "Fuel saving and other benefits of dynamic advisory speeds on a multi-lane arterial road," *Transportation Research Part A: General*, vol. 18, no. 5, pp. 421–429, 1984.

[43] A. Vahidi and A. Sciarretta, "Energy saving potentials of connected and automated vehicles," *Transportation Research Part C: Emerging Technologies*, vol. 95, pp. 822–843, 2018.

[44] A. Alessandrini, A. Campagna, P. D. Site, F. Filippi, and L. Persia, "Automated vehicles and the rethinking of mobility and cities," *Transportation Research Procedia*, vol. 5, pp. 145–160, 2015. SIDT Scientific Seminar 2013.

[45] Z. Zhang, Y. Zou, X. Zhang, and T. Zhang, "Green light optimal speed advisory system designed for electric vehicles considering queuing effect and driver's speed tracking error," *IEEE Access*, vol. 8, pp. 208796–208808, 2020.

[46] Z. Yang, Y. Feng, X. Gong, D. Zhao, and J. Sun, "Eco-trajectory planning with consideration of queue along congested corridor for hybrid electric vehicles," *Transportation Research Record*, vol. 2673, no. 9, pp. 277–286, 2019.

[47] H. Qi and X. Hu, "Bayesian inference of channelized section spillover via markov chain monte carlo sampling," *Transportation Research Part C: Emerging Technologies*, vol. 97, pp. 478–498, 2018.

[48] X. Wu, H. X. Liu, and D. Gettman, "Identification of oversaturated intersections using high-resolution traffic signal data," *Transportation Research Part C: Emerging Technologies*, vol. 18, no. 4, pp. 626 – 638, 2010.

[49] Y. Liu and G.-L. Chang, "An arterial signal optimization model for intersections experiencing queue spillback and lane blockage," *Transportation Research Part C: Emerging Technologies*, vol. 19, no. 1, pp. 130 – 144, 2011.

[50] E. Mintsis, E. I. Vlahogianni, and E. Mitsakis, "Dynamic eco-driving near signalized intersections: Systematic review and future research directions," *Journal of Transportation Engineering, Part A: Systems*, vol. 146, no. 4, p. 04020018, 2020.

[51] A. Dabiri, A. Hegyi, and S. Hoogendoorn, "Optimized speed trajectories for cyclists, based on personal preferences and traffic light information-a stochastic dynamic programming approach," *IEEE Transactions on Intelligent Transportation Systems*, pp. 1–17, 2020.

[52] S. Lin, B. De Schutter, Y. Xi, and H. Hellendoorn, "Efficient network-wide model-based predictive control for urban traffic networks," *Transportation Research Part C: Emerging Technologies*, vol. 24, pp. 122–140, 2012.

[53] H. Lim, W. Su, and C. C. Mi, "Distance-based ecological driving scheme using a two-stage hierarchy for long-term optimization and short-term adaptation," *IEEE Transactions on Vehicular Technology*, vol. 66, no. 3, pp. 1940–1949, 2017.

[54] S. Mandava, K. Boriboonsomsin, and M. Barth, "Arterial velocity planning based on traffic signal information under light traffic conditions," in *12th International IEEE Conference on Intelligent Transportation Systems*, pp. 1–6, 2009.

[55] B. Saerens and E. Van den Bulck, "Calculation of the minimum-fuel driving control based on pontryagin's maximum principle," *Transportation Research Part D: Transport and Environment*, vol. 24, pp. 89–97, 2013.

[56] B. HomChaudhuri and P. Pisu, "A control strategy for driver specific driver assistant system to improve fuel economy of connected vehicles in urban roads," in *2019 American Control Conference (ACC)*, pp. 5557–5562, 2019.

[57] N. Wan, A. Vahidi, and A. Luckow, "Optimal speed advisory for connected vehicles in arterial roads and the impact on mixed traffic," *Transportation Research Part C: Emerging Technologies*, vol. 69, pp. 548–563, 2016.

[58] H. A. Rakha, K. Ahn, K. Moran, B. Saerens, and E. Van den Bulck, "Virginia tech comprehensive power-based fuel consumption model: model development and testing," *Transportation Research Part D: Transport and Environment*, vol. 16, no. 7, pp. 492–503, 2011.

[59] M. W. Hancock and B. Wright, *A policy on geometric design of highways and streets*. American Association of State Highway and Transportation Officials, Washington, DC, 2013.

[60] J. P. T. van der Gun, A. J. Pel, and B. van Arem, "The link transmission model with variable fundamental diagrams and initial conditions," *Transportmetrica B: Transport Dynamics*, vol. 7, no. 1, pp. 834–864, 2019.

[61] P. A. Lopez, M. Behrisch, L. Bieker-Walz, J. Erdmann, Y.-P. Flötteröd, R. Hilbrich, L. Lücken, J. Rummel, P. Wagner, and E. Wießner, "Microscopic traffic simulation using sumo," in *The 21st IEEE International Conference on Intelligent Transportation Systems*, IEEE, 2018.

[62] A. Wegener, M. Piórkowski, M. Raya, H. Hellbrück, S. Fischer, and J.-P. Hubaux, "Traci: An interface for coupling road traffic and network simulators," in *Proceedings of the 11th Communications and Networking Simulation Symposium*, CNS '08, (New York, NY, USA), p. 155–163, Association for Computing Machinery, 2008.

[63] J. Hu, Y. Shao, Z. Sun, and J. Bared, "Integrated vehicle and powertrain optimization for passenger vehicles with vehicle-infrastructure communication," *Transportation Research Part C: Emerging Technologies*, vol. 79, pp. 85–102, 2017.

[64] SWOV, "Headway times and road safety," tech. rep., The Netherlands, 2012.

[65] S. Krauß, "Microscopic modeling of traffic flow: Investigation of collision free vehicle dynamics," tech. rep., Germany, 1998.

[66] A. Forde and J. Daniel, "Pedestrian walking speed at un-signalized midblock crosswalk and its impact on urban street segment performance," *Journal of Traffic and Transportation Engineering (English Edition)*, vol. 8, no. 1, pp. 57–69, 2021.

[67] G. Mahler and A. Vahidi, "An optimal velocity-planning scheme for vehicle energy efficiency through probabilistic prediction of traffic-signal timing," *IEEE Transactions on Intelligent Transportation Systems*, vol. 15, no. 6, pp. 2516–2523, 2014.

Glossary

List of Acronyms

PSC	predictive speed control
SPaT	signal phase and timing
I2V	infrastructure-to-vehicle
KWT	kinematic wave theory
FD	fundamental diagram
VT-CPFM	Virginia Tech Comprehensive Power-based Fuel Model
MPC	model predictive control
SUMO	Simulation of Urban MObility
CACC	cooperative adaptive cruise control